Distinct neural adaptations to time demand in the striatum and the hippocampus

Felipe Rolando, Tadeusz W. Kononowicz, Jean-René Duhamel, Valérie Doyère, Sylvia Wirth

Distinct neural adaptations to time demand in the striatum and the hippocampus

Felipe Rolando[1], *felipe.rolando@isc.cnrs.fr*

Tadeusz Kononowicz[1,2], *t.w.kononowicz@icloud.com*

Jean-René Duhamel[1], *jrd@isc.cnrs.fr*

Valérie Doyère[2], *valerie.doyere@universite-paris-saclay.fr*

and Sylvia Wirth[1], *sylvia.wirth@isc.cnrs.fr (lead contact)*

1. Institut des Sciences Cognitives Marc Jeannerod, CNRS, Université Lyon 1, 67 boulevard Pinel, 69500, Bron, France

2. Université Paris-Saclay, CNRS, Institut des Neurosciences Paris-Saclay (NeuroPSI), 91400 Saclay, France.

SUMMARY

How do neural codes adjust to track time across a range of resolutions, from milliseconds to multi-seconds, as a function of the temporal frequency at which events occur? To address this question, we studied time-modulated cells in the striatum and the hippocampus, while macaques categorized three nested intervals within the sub-second or the supra-second range (up to 1s, 2s, 4s or 8s), thereby modifying the temporal resolution needed to solve the task. Time-modulated cells carried more information for intervals with explicit timing demand, than for any other interval. The striatum, particularly the caudate, supported the most accurate temporal prediction throughout all time ranges. Strikingly, its temporal readout adjusted non-linearly to the time range, suggesting that the striatal resolution shifted from precise millisecond to coarse multi-second range as a function of demand. This is in line with monkey's behavioural latencies which indicated they tracked time until two seconds, but employed a coarse categorization strategy for durations beyond. By contrast, the hippocampus discriminated only the beginning from the end of intervals regardless of the range. We propose that the hippocampus may provide an overall poor signal marking an event's beginning, whereas the striatum optimizes neural resources to process time throughout an interval adapting to the ongoing timing necessity.

Keywords: Ongoing timing; Neural population dynamics; Temporal range adaptation; Striatum; Hippocampus

INTRODUCTION

We manage time differently depending on pressure, unaware of the passage of time when preparing for a distant event or attentive to time when this event is close. How does the brain track time when subjected to different timing necessities? Although involved in different cognitive functions, such as actions and habits on the one hand, episodic memory and navigation on the other hand, both the striatum and the hippocampus display time-modulated neural activity[1 2 3]. Similar neural patterns in the striatum and hippocampus were described when animals tracked a duration [1 4 5 6 7]. However, it is unknown whether and how both regions contingently adapt neural codes to track serial durations in ranges from the milliseconds to multi-seconds**.** To address this question, we analyzed neural activity in both regions in rhesus macaques performing a novel time-categorization task. Animals categorized three ongoing continuous durations, with two (short, intermediate) nested in the longer one, at the millisecond (up to 1s) or multi-second range (up to 2, 4 or 8s). The task therefore introduced different timing necessities through high to low temporal densities, with categorizations required at the level of the millisecond or the second depending on the sub-second, second or supra-second ranges. To ensure that the animal focused on potential time signals *per se*, the task did not rely on evaluation of the duration of a visual or auditory stimulation, nor of motor production, but response choices depended solely on the estimation of elapsed time since a brief cue. Our results identify for the first-time important differences in the time-modulated populational activity between the striatum and the hippocampus. We show that the striatum provides a stronger signal adjusting the precision of the time read-out from narrow to broad as a function of timing necessity, whereas the hippocampus only provides a poor time read-out at all time ranges. These results show how the brain adjusts neural resources differentially to time demands within different circuits.

RESULTS

Better performance for higher temporal demand

We recorded single-unit activity in the striatum and the hippocampus while two rhesus macaques performed a novel time-categorization task based on cumulative elapsed time, nesting two successive durations (short: 1/4, intermediate: 1/2) into a longer one (1/1, Figure 1A, STAR Methods). Monkeys were tested on different ranges, with the long duration ranging from 1 to 8 seconds on different blocks, thereby producing high-to-low density of stimuli

expectation within a single second across different time ranges (Figure 1B). Both monkeys categorized the three intervals well above chance (0.33) at all ranges (Figure 1C, $\chi^2(6)=3.3194e4$, $p<0.0001$ for Monkey#1; $\chi^2(6)=2.6883e4$, $p<0.0001$ for Monkey#2). Behavioural accuracy was globally higher at the sub-second (set 1s-long) and second (set 2s-long) ranges, followed by supra-second ranges: sets 4s-long and 8s-long. Within sets, the long interval was better discriminated at all ranges, except for the sub-second range, in which the short interval was better discriminated (Figure 1C, STAR Methods). Thus, monkeys performed the task well from sub-second to supra-second ranges, but there was a range-dependent decrease of performance, and potentially an effect of training history (STAR Methods), as the set 2s-long was the best categorized for both monkeys. The analysis of the nature of errors illustrates that animals were more likely to categorize an intermediate interval as long at supra-second ranges than at shorter ranges (Figure 1D, 1-way ANOVA $F(3,6384)=252.94$, $p<0.0001$). This latter result suggests that the monkeys' responses were not skewed toward shorter durations, hence, not driven by a preference for earlier rewards. On the contrary, it suggests that beyond 2 seconds, animals tended to overestimate time consistent with a categorical response rather than a time estimation. This goes against the previously documented effective strategy for motor production tasks, where responses are based on a prior distribution centered on the mean[8]. Interestingly, not only was the intermediate duration overall categorized less accurately, but the nature of the errors revealed underestimation in the 1s- and 2s-long sets, contrary to what would have been expected if the animals followed the intervals' means (0.583s, 1.166s, 2.333s and 4.666s for sets 1s-, 2s-, 4s- and 8s-long, respectively.). This lower accuracy for intermediate trials suggests that monkeys performed the task using a categorical rule distinguishing between 'short', 'intermediate', and 'long' resembling behaviour in a bisection task where categorization is better for the extreme values[9 10].

Two additional results demonstrated that monkey's behaviour did not exhibit scalar property in this task. First, the probability to respond 'long' differed between ranges for both monkeys (Figure 1E, 1-way ANOVA $F(3,331)=14.53$, $p<0.0001$ for Monkey#1, $F(3,314)=60.89$, $p<0.0001$, for Monkey#2, STAR Methods). Additionally, the Coefficient of Variation (CV) by blocks (Figure 1F), differed significantly for both, time range (2-way ANOVA, $F(3,1308)=112.71$, $p<0.0001$, STAR Methods) and interval ($F(2,1208)=95.52$, $p<0.0001$). The interaction

(F(6,1308)=20.13, p<0.0001) shows that CVs for short and intermediate intervals decreased with time range, while they did not do so for long intervals. Hence, temporal behaviour can undergo non-scalar adaptations likely driven by the specific task categorization demand. Second, normalized response latencies (STAR Methods, Figure 1G) were overall shorter at sub-second and second ranges. Moreover, there was a significant shift in distribution towards negative values for sub-second and second ranges, suggesting that the animals were better prepared to respond (at the end of any interval) at these ranges compared to longer ones. In addition, at short time ranges (less than 2s), responses were faster for the longest intervals, while at longer ranges (4s, 8s), they were slower for long intervals. As the task does not rely on the animal's speed to respond, this likely reflects a lack of motor preparation and a more passive waiting strategy, instead of active timing, for longer ranges. It could also reflect a slower decision-making process due to increased task difficulty, in line with the decreased performance for longer ranges. Importantly, the trial was aborted if any joystick movement was executed before the end of the interval instead of during the response window. Aborted trials were rare (less than 1.5% for Monkey#1, and less than 4.5% for Monkey#2), and their timing was consistent with an anticipation of the longest interval at the sub-second and second ranges. Therefore, the task likely dissociates evaluation of elapsed time from motor production providing a new way to assess time processing in rhesus macaques from milliseconds to multiple seconds. Overall, monkeys' performances were higher for finer categorization at the sub-second and second ranges, compared to supra-second ranges, in line with the hypothesis that temporal processing adjusts to temporal demand.

A strong recruitment of striatal cells that adapts to processing demand over time

To determine whether neurons displayed time-modulated signals, we analysed the spiking activity of 615 neurons in the caudate, 736 in the putamen and 929 neurons in the hippocampus (Figure 1H, STAR Methods). Analyses were computed on correct long trials, because short and intermediate durations were embedded into the longer one. We computed a time "Information Content"[11] (IC, in bit per spike) for the longest interval of each range partitioned in 100 bins. We defined time-modulated cells (TM cells) as cells for which the IC computed on actual data was above the 95th percentile of the distribution obtained from 1000 surrogates with permuted spikes (STAR Methods). TM cells (Figure 1I and Figure 2 for individual examples) were significantly more numerous in the caudate, followed by the

putamen and the hippocampus across all ranges (χ^2-test ran on each range, $\chi^2(3)=41.05$, $p<0.0001$, for set 1s-, $\chi^2(3)=117.78$, $p<0.0001$, for set 2s-, $\chi^2(3)=20.75$, $p=0.003$ for set 4s-, $\chi^2(3)=11.35$, $p=0.0034$ for set 8s-long, Figure 1G left pies). The percentage of TM cells remained approximatively constant across ranges within regions. There were only modest differences in the number of TM cells recruited between monkeys (Figure S1A) and the neural populations of TM cells in each monkey appeared strikingly similar (Figure S1B). To test whether the proportion of TM cells adapted to time demand, we compared the percentage of TM cells obtained from a fixed bin size and number (100x10ms) on a fixed interval (*i.e.* the first 1s, STAR Methods) across ranges. This method identified TM cells using only the first second of all possible ranges, the difference being the processing demand as a function of temporal expectancies during this first second (STAR Methods). The results showed that the percentage of TM cells identified for the first 1s at the second and multi-second ranges decreased dramatically in the striatum, compared to the number of cells identified when one second is the long interval (Figure 1I right pies, $\chi^2(2)=63.4434$, $p<0.0001$ in caudate, $\chi^2(2)=21.5167$, $p<0.0001$ in putamen), but not in the hippocampus ($\chi^2(2)=5.95$, $p=0.051$). In sum, while hippocampal activity displays very little time-related changes, striatal activity, especially in the caudate, is strongly modulated, and further, time within intervals is processed adaptively relative to time range and temporal expectancies.

A mix of ramping and sequential peaks across brain areas

The nature of neural activity throughout time has been linked to different computational functions[12]. For example, peak activity can represent precise temporal boundaries[9] or expected stimuli[13]. Here, we hypothesized that cells peaked near expected events, *i.e.* the potential interval ends (red lines in Figure 2). However, visual inspection of activity through time (Figure 2 for 2s-long interval, and Figure 3A and Figure S1B for population time maps) revealed a variety of time-modulated patterns that did not specifically fit these expectations. Via a stepwise regression (STAR Methods), we identified a higher proportion of ramping neurons in the striatum compared to the hippocampus at all time-ranges (Figure S1C-D). An ANOVA on the absolute linear terms, confirmed a significant effect of regions: caudate and putamen exhibiting stepper slopes (*i.e.* more ramping activity) than hippocampus, but no effect of time range, nor interaction (Figure S1D, 2-way ANOVA, $F(2,677)=36.54$, $p<0.0001$ for region). In addition, the net changes in firing rate amplitude, computed on 20ms bins across

sets, differed between brain area (2-way ANOVA, $F(2,245.45)=13.45$, $p<0.0001$) and time range ($F(3,677)=19.14$, $p<0.0001$) with no interaction: amplitudes at the sub-second and second ranges were significantly higher than at the longer ranges. In sum, the TM cells in the caudate exhibited the highest changes in amplitude, linked with steeper slopes, followed by the putamen and then the hippocampus.

We then showed that peak activity was not homogeneously distributed within the long interval in any region at any time range (Figure S1E, STAR Methods). While many TM cells responded to reward delivery (Figure 2, Figure S1F), we found that it was not indicative of the peaks' distribution within the interval (Figure S1G), nor linked to reward valuation or expectation as a function of interval length. Only a minority of TM cells exhibited distinct responses to rewards depending on the interval (STAR Methods): 23.6% in the caudate (*n*=35/148) and 28.6% in the putamen (*n*=26/91). Instead, the majority of cells reached maximal firing rate within the first half of the trial in all the brain regions (Figure S1E), suggesting that TM cells carried more information during the part of the interval requiring more time processing demand, rather than relative to the upcoming reward. Finally, we tested whether "time field" size, known as the width, increased as a function of peak-times as previously reported[9 14 7 15], within and across ranges. Width did not increase within a time range' interval (Figure S1E), but increased with the overall size of the interval with increasing time-ranges (Figure S1H). This suggests an effective neuronal recruitment adjusting "time field" density to time demand.

Little involvement of striatal TM cells in motor preparation and execution.

In addition to reward evaluation, the striatum is intricately engaged in movement execution and preparation[16 17 18]. In our task, we found that only a small fraction of neurons displayed selectivity for a specific movement during execution after the interval's end (STAR Methods, Figure S1F, third row): 37.2% of caudate neurons (*n*=55/148) and 39.6% of putamen neurons (*n*=36/91) exhibited exclusive preference for a single movement at the second range.

Then, we asked whether the pattern of neural activity during the interval could be linked to the movement preparation itself, focusing on TM cells recorded during both the 1s-long and 2s-long sets in the caudate (*n*=87) or the putamen (*n*=38). Our rationale was that, if neurons prepared for a specific movement, their activity before a motor action (e.g., classifying the interval as 'short' at sub-second or second ranges) should remain consistent

across different time ranges. In the caudate, 24% of cells (21/87) were not influenced by movement (Figure S2, top row). Next, 71% of cells (62/87) were modulated by upcoming movement, but the majority of these (39/62) was also modulated by time range, (Figure S2, middle row). In the end, only 23 neurons (26.4%) were modulated by upcoming movement only, without any effect of time range (Figure S2, bottom rows). These neurons may potentially be candidates for motor preparation rather than explicit time computation. However, they constitute a minority within the neural population.

In the putamen, following a similar breakout, 26.3% of neurons (10/38) were unaffected by movement Among the 58% of cells (22/38) influenced by movement, 31% (12/38) were also modulated by time range. Only 26.3% of neurons (10/38) exhibited a significant movement, devoid of any time-range impact or interaction. Thus, akin to the caudate, only a few neurons in the putamen might reflect motor preparation, independent of time range.

A slow speed but steady progression of a circular neural trajectory in the caudate

The population's activity in all regions presented dynamic changes over time (Figure 3A). It was proposed that such neural dynamics constitute distinct states through time[19 20 21] of a moment-to-moment trajectory in a neural space. The population's activity is then represented in an "*n*" dimensional space, as a function of *n* neurons, over the number of time-bins "*t*", and captured through dimension reduction techniques such as principal component analysis (PCA), represented in Figure 3B, via the projections of the first two principal components (PCs). Strikingly, the first PCs revealed a circular progression strongly separating neural states through time in the caudate and putamen, while this is less clear in the hippocampus. To directly compare neural trajectories across regions and time ranges (Figure S3C,D,G), we employed a down-sampling method (STAR Methods) computing PCs on equal-sized subsamples obtained on each iteration. First, we determined that fewer components captured 50% of the variance in the caudate compared to other regions at all time-ranges (Figure S3A). The lower dimensionality at short time range (less than 5PCs) compared to higher dimensionality at longer time range (less than 11 PCs) suggested that stronger time representation (such as at short time range) is associated to a low dimensional space, confirming previous results[22]. Second, using an absolute binning method (STAR Methods), we computed: a) the distance between the neural state at each time-bin and the centroid of the

trajectory (Figure 3C and S3B,D,F x-axis), and b) the instantaneous Euclidean distances between two consecutive time-bins (Figure 3C and S3B,D,F, y-axis), referred to as the speed of the neural trajectory[6] (STAR Methods). The overall distance was larger in the caudate, followed by putamen and hippocampus (2-way ANOVA, $F(2,2238)=9.8$, $p=0.0001$), and decreased significantly as time range increased ($F(2,2238)=58.35$, $p<0.0001$), with no interaction between the two factors (Figure S3B-D-F). The average speed was significantly different 1) between regions, lower for caudate followed by putamen, and then hippocampus (Figure 3C, 2-way ANOVA, $F(2,11988)=45012.44$, $p<0.0001$); and 2) across ranges (Figure 3D), with an overall higher speed at sub-second range ($F(3,11988)=20076.29$, $p<0.0001$) dominated by smaller speeds in the caudate compared to other regions ($F(6,11988)=7903.57$, $p<0.0001$). In sum, low speed, coupled with a large distance from the centroid, reveals a neural trajectory occupying a larger area despite small alterations between consecutive time-bins. To test whether speed displays a scalar adaptation across ranges, we computed a Coefficient of Variation (CV, STAR Methods). Within each region, the CVs were strikingly different from sub-second and second ranges to supra-second ranges (Figure 3E, 2-way ANOVA, $F(6,11988)=17.2798$, $p<0.0001$). This suggests that the variation of speed from a time range to another was not scalar[23].

Finally, to capture the dynamics in the PCs space over time across regions, using a relative binning method, we computed the angular position of each time-bin with respect to the centroid (crosses in Figure 3B) and then, calculated the moment-to-moment differences between the angles obtained for consecutive time-bins (STAR Methods). Figure 3F represents the distribution of 1000 angles obtained on the subsamples from the 1000 iterations for each of the 100 time-bins at the second range (Figure S3C-E-G for other ranges). The moment-to-moment changes incremented more linearly in the caudate and putamen compared to hippocampus (2-way ANOVA, $F(2,1176)=102.27$, $p<0.0001$, STAR Methods). There was a significant effect of the range ($F(3,1176)=12.72$, $p<0.0001$), but the interaction ($F(6,1176)=9.55$, $p<0.0001$) revealed this was mainly driven by the hippocampus, which displayed no overall increments at set 1s- and set 8s- compared to set 2s- and 4s-long (Figure S3). Together with measures of speed and distance in trajectory over time, the results show that the caudate, followed by the putamen, exhibited dynamics made of large, steady and continuous changes in moment-by-moment population states through time, without

exhibiting *temporal scaling in speed nor strong changes in geometry across ranges.* On the contrary, the hippocampus exhibited disorganized changes through time. The results suggest that striatum neural trajectory may better support a continuous time read-out than the hippocampus.

Neural trajectory analysis reveals non-scalar time encoding in caudate activity

The changes in speed across different time ranges suggest that the trajectory adapts as a function of time demand, which may occur without changing the overall geometry. We reasoned that if time is encoded in an absolute way, then, neural trajectories should progress at the same speed on an absolute scale for different time ranges. On the other hand, if the end of a trajectory represents a category to reach (e.g. long), the speed would adaptively rescale in a relative manner. To test these hypotheses, we performed a PCA on the 87 caudate TM cells activity, concatenating the two time ranges, using a 20ms binning and a bootstrapping method (STAR Methods). Figure 4A shows the scores obtained at each iteration for each time sample for 1s-long in purple (top) and for 2s-long in orange (bottom). We considered rescaling (Figure 4B, left) and no rescaling hypotheses (Figure 4B, right), by computing distances between trajectories according to an absolute or relative sampling (STAR Methods). The linear regressions of these distances are represented in Figure 4C (dashed lines for the fit average and shaded areas for standard deviation). The slopes were significantly higher for the absolute sampling (1-way ANOVA, $F(1,1908)=2507.14$, $p<0.0001$) indicating the presence of rescaling. In addition, 97.7% of the regressions computed on the 1000 absolute samplings were significant, while this was the case for only 36.13% of the regressions computed on the relative samplings. In sum, the distances between PCs for 1s and 2s obtained through absolute and relative samplings matched the relative rescaling prediction (Figure 4C), indicating that the neural trajectory rescaled time within the interval.

To test the nature of the rescaling, we compared the final positions of the neural trajectories between ranges (Figure 4D), assuming these wouldn't differ if the rescaling was scalar. However, the distribution of the final PC scores differed significantly for PC1 (2-sample T-Test, T-stat(1953)=-7.8466, $p<0.0001$) and PC2 (T-stat(1953)=-29.5397, $p<0.0001$), suggesting that the final positions did not overlap. However, we then showed that the distribution of scores of the end of the 1s-long interval did not overlap either with the ones for the half of the 2s-long interval (PC1 scores, 2-sample T-Test, T-stat(1953)=-115.4932,

p<0.0001; PC2 scores, T-stat(1953)=95.2070, p<0.0001, Figure 4E), confirming a rescaling pattern. Therefore, the results indicate that the neural activity of the caudate rescales the durations between the second and sub-second ranges. Yet, because the final positions did not overlap, the neural adjustments do not appear to follow "scalar" rules, despite being scalable.

Neural activity supports explicit time processing demand

We compared the strength of time prediction between regions with a decoder based on linear regression (STAR Methods). First, in any region, only decoding based exclusively on TM cells was significantly higher than chance (Figure 5A). Next, we asked whether the temporal organization of neural activity within the timed interval was unique to that specific interval, or whether it allowed decoding time in another interval. To address this, we trained a model on the first 800ms of the 2s-long interval (coloured in Figure 5B) and then compared i) the predictions generated when tested with these 800ms, and ii) the predictions generated when tested on the 800ms of the inter-trial interval (ITI, in grey in Figure 5B). Decoding was above chance when tested on the first 800ms of the interval in the striatum only (p=0.0008 for caudate and p=0.0038 for putamen), but was not significantly different from chance when tested on the ITI. Thus, the neural organization within the interval was unique to the timed interval, and could not support time decoding during the ITI. We then asked whether TM cells activity could support time decoding for other periods (STAR Methods). TM cells identified during the timed interval did not support time decoding for another interval (Figure S4A). However, in theory, another interval could be timed by a different subpopulation of neurons. Thus, we identified TM cells during the ITI (instead of the timed interval, STAR Methods). We found fewer TM cells during the ITI than during the timed interval: 34 neurons in the caudate (7.38%), 51 (8.89%) in the putamen and 51 in the hippocampus (6.74%). We used these neurons to test the decoding during the ITI (Figure S4B), assuming that they were more likely to decode time during ITI than TM cells defined during the timed interval. Strikingly, time of the ITI could not be predicted above chance with these populations (p=0.146 in caudate, p=0.0922 in putamen, p=0.2729 in hippocampus). In sum, the key finding is that the striatum and the hippocampus did not support time *per se*, but rather only time within the temporal window needed to solve the task.

A time prediction in the striatum maintained across multiple time ranges

To test whether the strength of time prediction varied across time ranges, we down-sampled neural populations to enable a comparison across regions (Figure 5C, STAR Methods). By comparing regressions obtained at each iteration (top insets in Figure 5C), we found that decoding based on both striatal regions performed above chance at all time-ranges, unlike hippocampal-based decoding (p=0.0008, p=0.0022, p=0.0248 and p=0.0078 for caudate, respectively at sets 1s-, 2s-, 4s- and 8s-long and p=0.0028, p=0.0216, p=0.0054 and p=0.0472 for putamen). Further, the distances of the predicted time to the real time at each time-bin and across time ranges, (bottom insets in Figure 5C) revealed better time prediction in the caudate compared to the putamen, while hippocampal-based prediction was very poor (2 way ANOVA, $F(2,1188)=96.83$, $p<0.0001$). Across time ranges, striatal-based decoding performances decreased only at supra-second ranges ($F(3,1188)=6.27$, p=0.0003). The interaction ($F(6,1188)=3.75$, p=0.001) revealed that caudate-based predictions were better than putamen's, specifically at the longer range. Overall, the results underscore the higher suitability of caudate neural activity to predict time over putamen and hippocampus.

Discriminability between two time-points adapts to processing demand from milliseconds to supra-second ranges

The regression-based analysis assesses overall strength of temporal prediction but doesn't characterize the precision of the moment-to-moment discrimination within the interval. Hence, to characterize the temporal resolution, we used Support Vector Machine (SVM)-based decoding on each possible pair of time-bins within an interval (STAR Methods). Figure 6A shows the results as a time-by-time matrix, where each pixel is the discrimination probability (accuracy) between two time-points of the interval, t_n and t_m. First, average accuracy (Figure 6B) was higher in the caudate, followed by the putamen, then the hippocampus (2-way ANOVA, $F(2,59388)=5876.61$, $p<0.0001$). Across time ranges, accuracy was slightly better in the well-trained second range interval than at sub-second range, but decreased strongly for longer intervals ($F(3,59388)=3517.73$, $p<0.0001$). The significant interaction ($F(6,59388)=399.83$, $p<0.0001$) indicates a faster decrease of accuracy beyond the second range in the caudate, than in putamen.

Next, to test whether changes in decoding accuracy within the interval were indicative of categorical representations (short, intermediate or long), we conducted an unsupervised clustering analysis (K-means analysis) on the time-by-time decoding accuracy. The clusters obtained did not correspond to distinct time intervals, and their number (Figure S5A) far exceeded the actual number of expected events (*i.e.* 3) in any region. Rather, the number of clusters was inversely proportionate to decoding accuracy, with fewer clusters observed in the striatum compared to the hippocampus. This observation reflects a lower time-by-time variability in the striatum.

To quantify decoding accuracy for each time-bin, we calculated its discriminability score (ranging 0 to 99,STAR Methods, Figure 6C). In the striatum, discriminability scores were overall higher than chance during the whole interval. Within short intervals, discriminability scores were maintained at a very high level throughout, as indicated by the null or close to zero slopes at sub-second range (β_1=-0.0172, p=0.3361 for caudate; β_1=-0.0973, p<0.0001 for putamen), or at the second range (β_1=-0.0727, p<0.0001 for caudate; β_1=0.0164, p=0.1786 for putamen). This contrasted strongly with the steep decrease observed for longer intervals (at 4s-long, β_1=-0.5416, p<0.0001; β_1=-0.2964, p<0.0001, respectively for caudate and putamen; and β_1=-0.3452, p<0.0001; β_1=-0.4905, p<0.0001 at 8s-long). This suggests that in the striatum, unlike a categorical representation, time is continuously represented with the same strength within the interval throughout short time ranges, whereas at longer time ranges, the beginning is better discriminated from the rest of the interval. In the hippocampus, discriminability was maintained above chance for the entire interval only at the second range (the time range used for training, β_1=-0.2923, p<0.0001). At the sub-second range, only the very end of the interval was discriminated from the rest of the interval (β_1=0.3841, p<0001), whereas at longer ranges, discriminability was higher at the beginning of the interval and decreased steeply with time, as indicated by the strong negative slopes (β_1=-0.3561, p<0.0001; and β_1=-0.3871, p<0.0001 respectively for 4s-long and 8s-long ranges). This pattern illustrates a coarse temporal discrimination in the hippocampus at sub-second and supra-second ranges, which only discriminates beginning from end of intervals. In all regions, the steep decrease in discriminability score within the interval at long ranges suggests a temporal adaptation that was not scalar, as the accuracies were not equally distributed across time-ranges. These

results also align with the observation that temporal prediction decreased for longer time ranges (Figure 5C).

Next, we examined the temporal resolution of the decoding within and across ranges, defined as the distance t_i-t_j, where t_j is the closest time-bin from which t_i is decoded above chance (STAR Methods). A small to large distance reflects variation from fine to coarse temporal resolution, and can be intuitively perceived along the narrow to wide diagonals in Figure 6A. Overall, the resolution was narrower in the caudate and putamen than in the hippocampus (2-way ANOVA, $F(2,1188)=80.82$, $p<0.0001$), and widened with increased durations ($F(3,1188)=149.37$, $p<0.0001$). The post-hoc analysis following the significant interaction ($F(6,1188)=7.76$, $p<0.0001$) showed a difference between caudate and putamen at the 4s-long range only. Further, the caudate and putamen temporal resolution did not change from sub-second to second range, but widened significantly at supra-second ranges. An analysis of breaking points allowed excluding that temporal resolution adjusted in a step-wise fashion to anticipated events. We found more breaking points for the putamen and the hippocampus than for the caudate, but did not observe any evidence that these changes occurred at the expected events during the interval (1/4, 1/2 and 1) in any region (Figure S5B). Taken together, the results suggest that the temporal resolution for time was not categorical within an interval, and adapted to temporal demand across ranges, with a high resolution at sub-second and second ranges compared to a lower one at supra-second ranges. This adaptation did not appear to be scalar, as the resolution at different ranges differed when represented in a relative scale (Figure 6C).

The neural encoding of 1s is contextually adapted across ranges

Here, we compared decoding accuracy for the first 1s of the timed interval depending on the time range at which the animal performed. Importantly, while the cue onset was the same, the task relevant durations differed between ranges. We hypothesized that the decoding resolution adapted to the time processing demand and expected events (*e.g.* possible endings of trials at 0.25 or 0.5 for the set 1s-long, whereas no event was expected before 2s during set 8s-long). Therefore, we performed the pairwise decoding on the first 1s of the second- and supra-second ranges using the neurons defined as TM cells for this specific duration (Figure 1I, right pies). The first 1s was better decoded at sub-second and second ranges compared to supra-second ranges (Figure S5C, $F(3,59388)=3094.3$, $p<0.0001$) and caudate population

based decoding accuracy was above the other ones ($F(2,59388)=2491.44$, $p<0.0001$). The interaction ($F(6,59388)=881.48$, $p<0.0001$) confirmed the better decoding accuracy achieved by the striatum, mixed with lower decoding at supra-second ranges. Significant time decoding for the first second in the hippocampus was nearly absent at all ranges. In sum, in the striatum only, temporal accuracy was finely adapted to time demand.

DISCUSSION

By recording neural activity while non-human primates successfully categorize elapsed-time (Figure 1), we demonstrated distinct neural dynamics between striatum and hippocampus despite the presence of "time cells" in both regions (Figure 2). Hippocampus activity poorly signalled elapsed time. In contrast, many cells in the striatum were recruited by the task (Figure 1I). Striatal neural trajectory displayed a constant progression through time (Figure 3) which supported temporal prediction at all ranges (Figure 5C). The neural trajectories (Figure 3) and population-based temporal decoding adapted to the contextual time demand (Figure 5B, S4, S5C), yet in a non-scalar fashion (Figure 3E, 4). Specifically, the temporal resolution adjusted from milliseconds at the shorter ranges, to coarser multi-second resolution at supra-second ranges (Figure 6). In contrast, the hippocampus poorly represented moments by discriminating interval beginning from ending. The present evidence for differential adaptation for time in the striatum and the hippocampus, is a major cornerstone to understand how the brain adjusts neural resources to meet temporal demand within distinct circuits.

Neural tracking of time is selective to intervals requiring explicit timing.

Our study is the first to report accurate estimation of elapsed time below 2s and up to 8s in macaques, in a task that, unlike others, is not based on a timed motor production[24 25] or on a stimulus duration discrimination[26]. Striatal activity supported time representation specifically for the temporal window relevant to the task (*i.e.* the timed interval). This is seen in successful decoding from TM cells identified during timed interval only (Figure 5A) and not during intervals irrelevant to the task, such as the ITI (Figure 5B, S4), nor during the first second of longer durations (Figure S5C)., Such epoch specificity was also present in the hippocampus, despite poorer time decoding (Figure 5A). Therefore, time signals in both regions do not indicate elapsed time in general (time *per se*), but rather are recruited for explicit timing during

the temporal window relevant to the task. This suggests a cognitive control during time tracking exerted on both regions.

Striatal neural dynamics more suitable to temporal read-out than hippocampal dynamics.

We expected striatum activity to support temporal decoding[27 5 28 7 10]. In the hippocampus, "time cells" encoded sequence order at short time range[29], or specific moments in longer periods[30 1]. However, a direct comparison of time read-out based on striatal and hippocampal dynamics has never been reported. Further, whether neural activity in each region provided discrete encoding of multiple serial durations or a continuous representation of time was unknown. Here, we reveal large differences between these regions. While ramping cells were almost absent in the hippocampus, a mix of ramping and peak neurons was recruited in the striatum. The latter provided progressive and steady changes in neural trajectory through time (Figure 3F, S3), in line with results linking ramping activity with timing[22 31] and showing that highly distributed sequential peaks supports better time read out in rodent's striatum[5 28]. The idea that explicit timing is encoded within low-dimensional manifolds has been proposed[32 22]. Given the low number of PC explaining variance in the caudate, we speculate that this area offers the most suitable neural foundation for timing in this task, particularly excelling at shorter time intervals. Overall, our findings suggest that the striatum provides a continuous -not categorical- representation of time, despite the previously documented role of the putamen in sequential stimulus categorization[33 34].

Further, associated to the large striatal neural trajectories, population-based predictions were above chance up to 8s (Figure 5C) and overall higher in the caudate compared to the putamen, introducing herein a distinction within striatal territories, likely based on input[35 36 37] or specific functional organization within the cortico-striatal loops[38]. Indeed, compared to the putamen, the caudate has a stronger connectivity with dorsolateral and ventro-medial prefrontal cortex, orbito-frontal cortex and dorso-anterior cingulate cortex[16 39]. These brain regions are known to be involved in working memory[40 41], sequence learning[42], reward sequences[43] and reward discounting[44 45], which are cognitive functions heavily relying on precise time representation. Therefore, stronger timing signal may stem from the caudate's connectivity with these prefrontal regions. In contrast, the putamen is involved in motor-execution[17], motor-selection and habit learning[46], consistent with the regions' main inputs and outputs with motor area 4[47 37 48]. Thus, unlike the caudate, the

putamen is more suitable to support the execution of context-adapted movements[49 50 51]. Previous studies showed that inactivation of the caudate, but not the putamen, increased impulsivity[52]. Nonetheless, the functional distinction between the caudate and putamen remains contentious[16]. Surprisingly few studies compared neural activity in these regions, making our study an important step toward understanding their functional differences.

Starkly contrasting with striatum, disorganized hippocampal neural trajectories (Figure 3, S3) failed to support temporal prediction above chance. This is surprising considering the literature reporting high sequentiality provided by hippocampal "time cells" [53 54 55]. We also report "time cells", but the nature of hippocampal TM-based decoding, discriminating beginning from end of intervals, echoed the entorhinal "relaxation" cells, allowing higher temporal prediction for the beginning of an interval[56]. More broadly, our findings suggest that internally-generated sequences poorly support time representation in the absence of visual[57 29], sensory-motor[4 58 30] or social components[59].

Behaviour and neural activity adapt as a function of timing necessity

Do timing behaviour and time-modulated neural signals adapt in parallel to time demand? Animals transferred the time-based rule from one time range to another, suggesting that monkeys represented classes of relative durations within and across ranges (Figure 1C). However, monkeys transferred the rule better from the second to the sub-second range, compared to the supra-second ranges. The nature of errors suggested a subjective timing in which the internal clock's pace speeds up for longer time ranges, leading to overestimations of longer intervals (Figure 1D). Alternatively, time is less finely tracked beyond 2s, leading to threshold-based categorization (*i.e.* long once 2s is passed). Accordingly, response latencies indicated higher anticipation for intervals ending under 2s, at any time range, even when 2s was the longest interval (Figure 1G). In sum, the results suggest a non-scalar adaptation across time ranges (Figure 1E-F) supported by a transition in timing strategy from fine tracking for high temporal demand at shorter ranges, to coarse categorization at supra-second ranges. Neural activity in the striatum appeared to follow a parallel pattern. The read-out accuracy of striatal neurons adapts to temporal demand, high at short ranges and low at long ones (Figure S5C), by adjusting its temporal resolution in a non-scalar way (Figure 6). An analysis of the moment-to-moment changes in caudate neurons recorded across two time ranges (Figure 4), confirmed that the ratio of the change in speed of neural trajectory was not scalar. By contrast,

the hippocampus exhibited a poor and coarse representation of ongoing time, as illustrated by the low number of cells displaying time-related properties. This representation of time was stronger at the second range, likely because the animals were trained at this range, thus implying the hippocampus may be recruited for well-known durations[1].

The results showing a "non-invariant" adaptation in the striatum contrasts with studies showing scalar rescaling on seconds-to-minutes fixed-interval timing in rodents[60 7], or scalar trajectories adaptation for timed movement in macaques prefrontal cortex and caudate[6] or in medial premotor cortices[61]. Our findings also contrast with the striatal-beat frequency model, which proposes that the striatum reads out multiple pacemakers[62 63] and provides a precise and time-range invariant interval timing[64]. Several differences may explain the contradictions. First, in fixed-interval[60 7], bisection tasks[9 65], and motor-production[6 66] or -reproduction[31] tasks, when a trial starts, only one duration has to be estimated or produced. This is unlike our task, in which three nested intervals must be discriminated thereby varying event's temporal frequency and required timing precision. Thus, scalar scalability may be relevant to the anticipation of a single event, but less for multiple events within a short temporal window. Second, unlike previous neurophysiological studies of timing in animals, our task dissociated temporal estimation from motor production, as the motor response had to be performed after the timed interval had elapsed. Furthermore, our three nested interval task has inherent complexity which likely increased processing demand. Therefore, we suggest that scalar scalability may break down when the subjects process temporal expectancies of multiple successive events for which neural activity reflects the temporal density.

In sum, our results suggest that striatal neural time tracking adapted to timing necessity, while, hippocampal neural time remained more invariant. The striatum's range adaptation may be limited by biological constraints restricting short-term plasticity within the cortico-striatal network[67]. This may reduce the delay allowing associating the neural sequence recruited at the beginning of the interval and the feedback received at the end of the interval. We suggest that feedback at short or long delays provides an intrinsic way to flexibly modify neuronal resources as a function of time demand, across various ranges.

Acknowledgements

This project was supported by ANR-17-CE37-0014 Time-Memory grant and LABEX CORTEX. We wish to thank Serge Pinède for technical support, and Fidji Francioli and the animal facility staff for animal care. We also thank Charles Wilson and Virginie van Wassenhove for useful discussions and Lawrence Parsons for proofreading and editing the English.

Author contributions

S.W. and V.D. conceived the project. S.W., V.D., J.R.D and F.R. designed the task. F.R. collected the behavioural and the electrophysiological data. T.K. implemented the pair-wise decoding analysis. F.R. performed all other data analysis. F.R. analysed the data with contributions from T.K., V.D. and S.W. F.R and S.W. interpreted the data and wrote the manuscript. S.W. supervised the project. All authors contributed to the writing of the manuscript.

Declaration of interest

The authors declare no competing interest.

552

553 Figure1

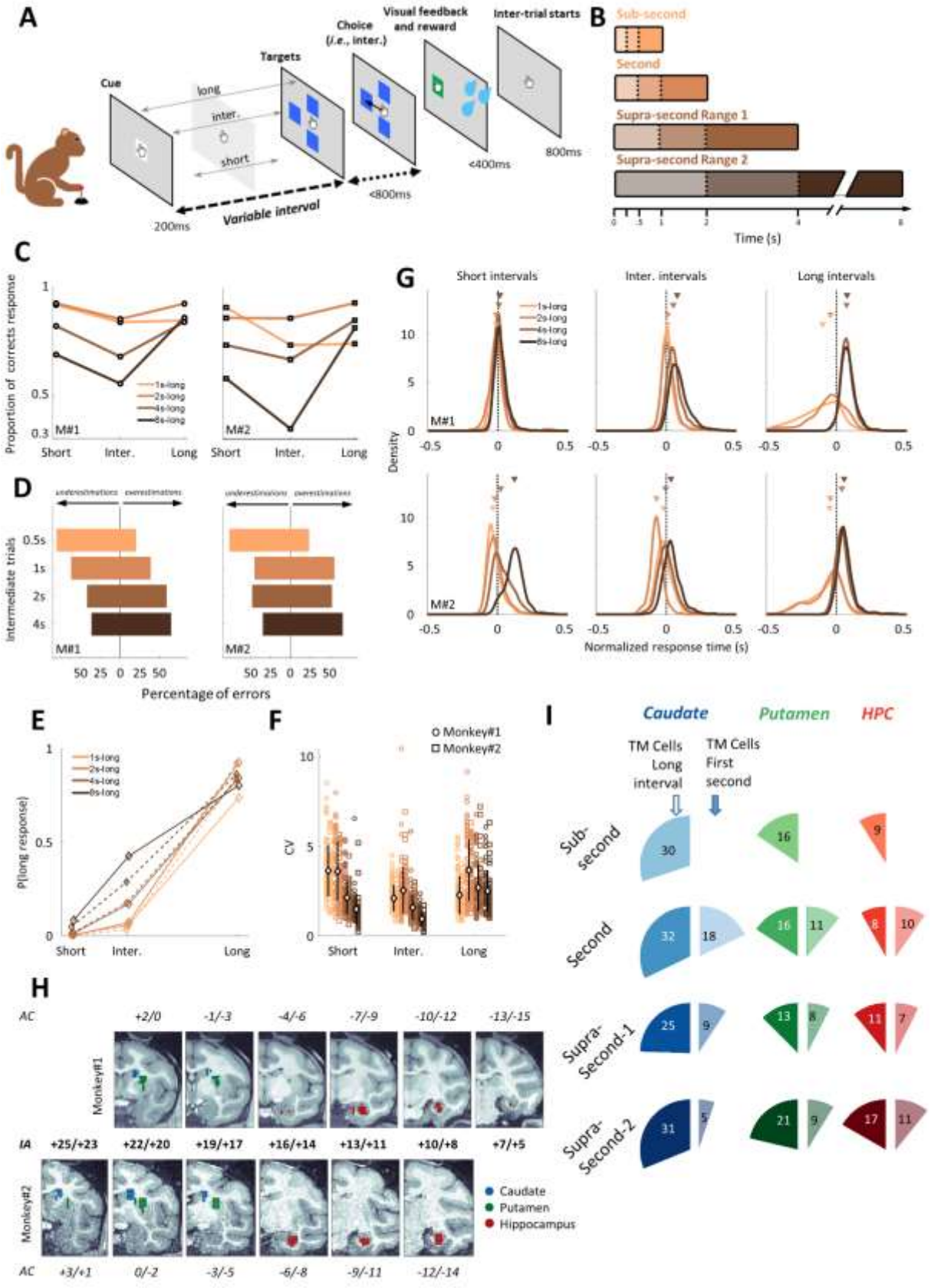

554

555 Figure 2

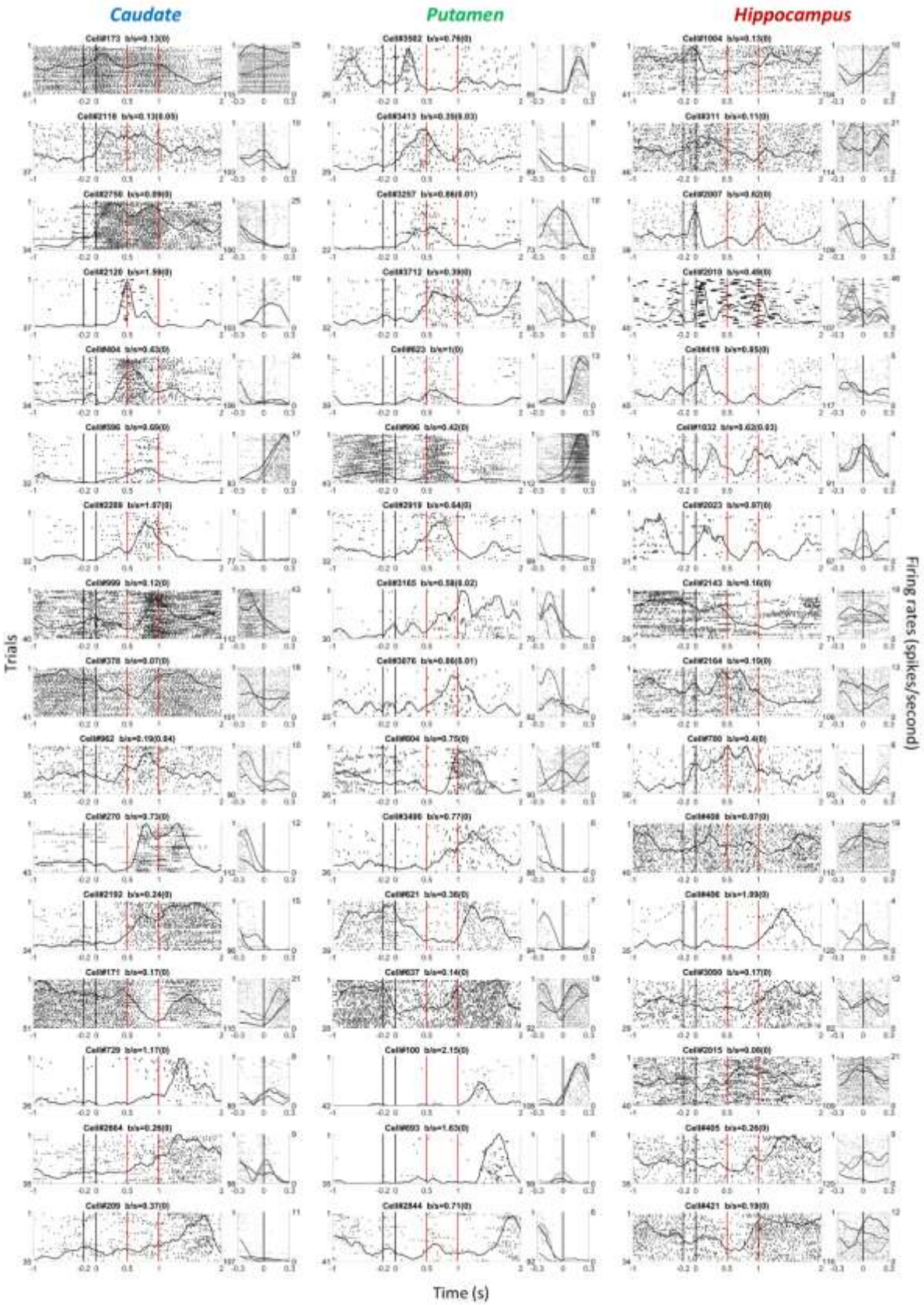

556

557

Figure 3

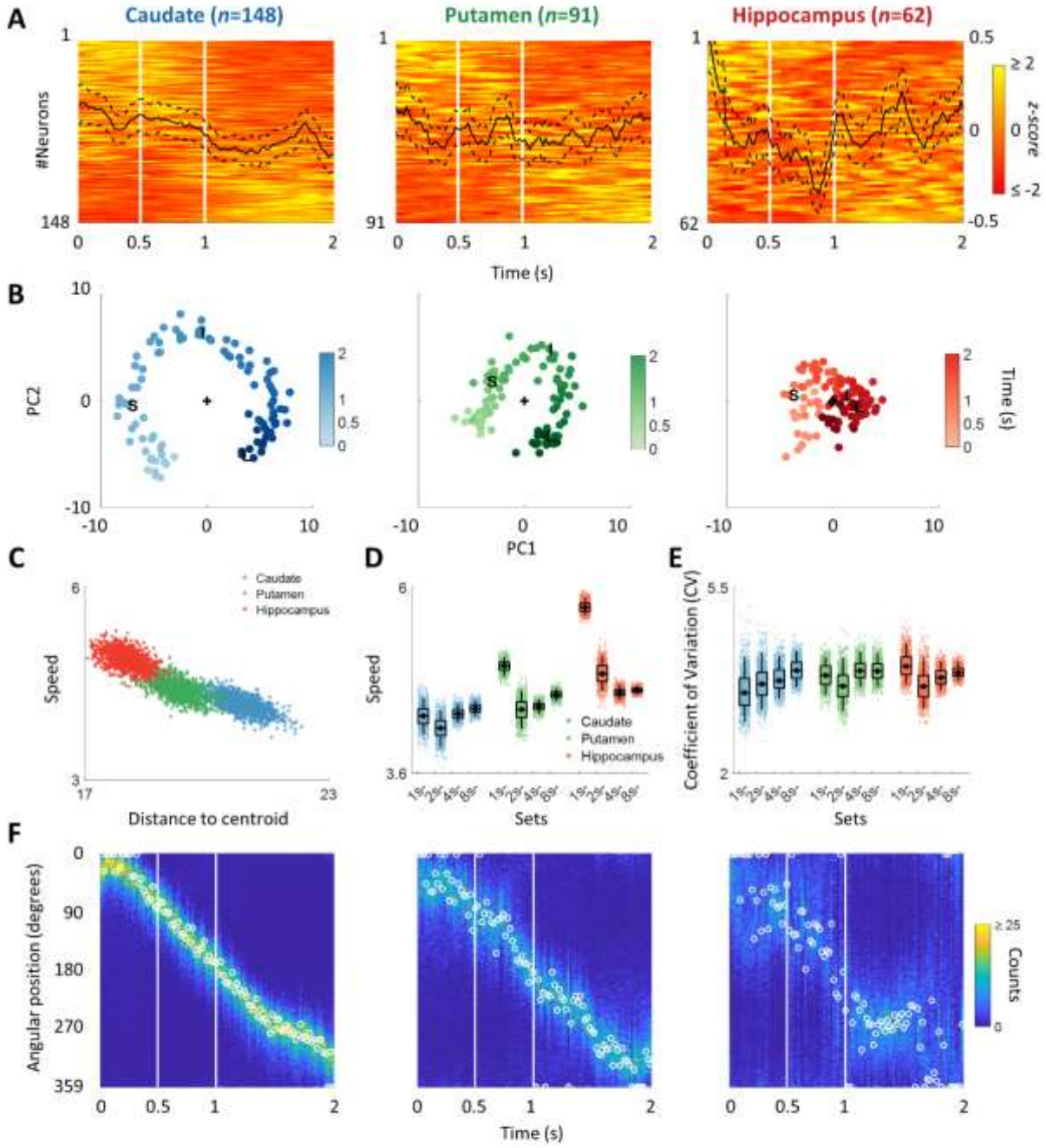
A
Caudate (n=148)
Putamen (n=91)
Hippocampus (n=62)
#Neurons
z-score
Time (s)
B
PC2
PC1
Time (s)
C
Caudate
Putamen
Hippocampus
Speed
Distance to centroid
D
Speed
Sets
E
Coefficient of Variation (CV)
Sets
F
Angular position (degrees)
Counts
Time (s)

561 Figure 4

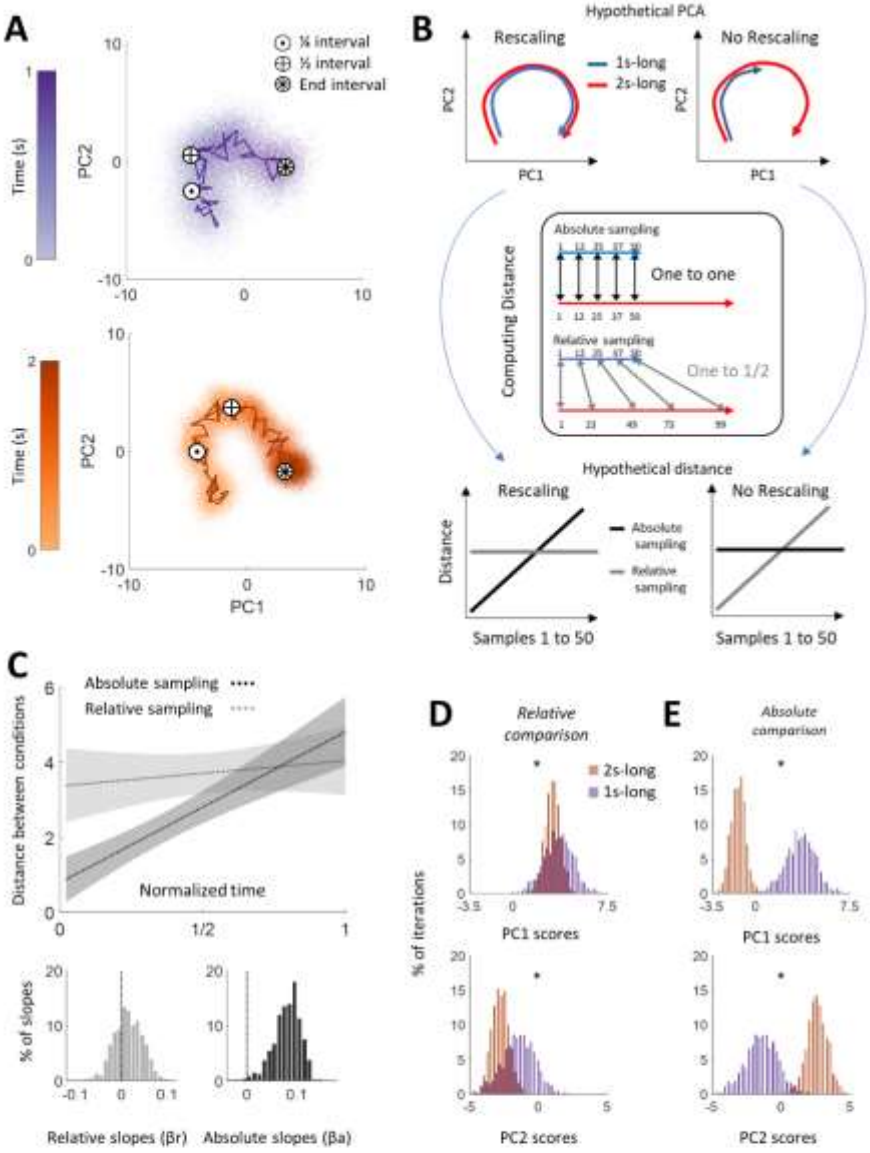

562

563

564 Figure 5

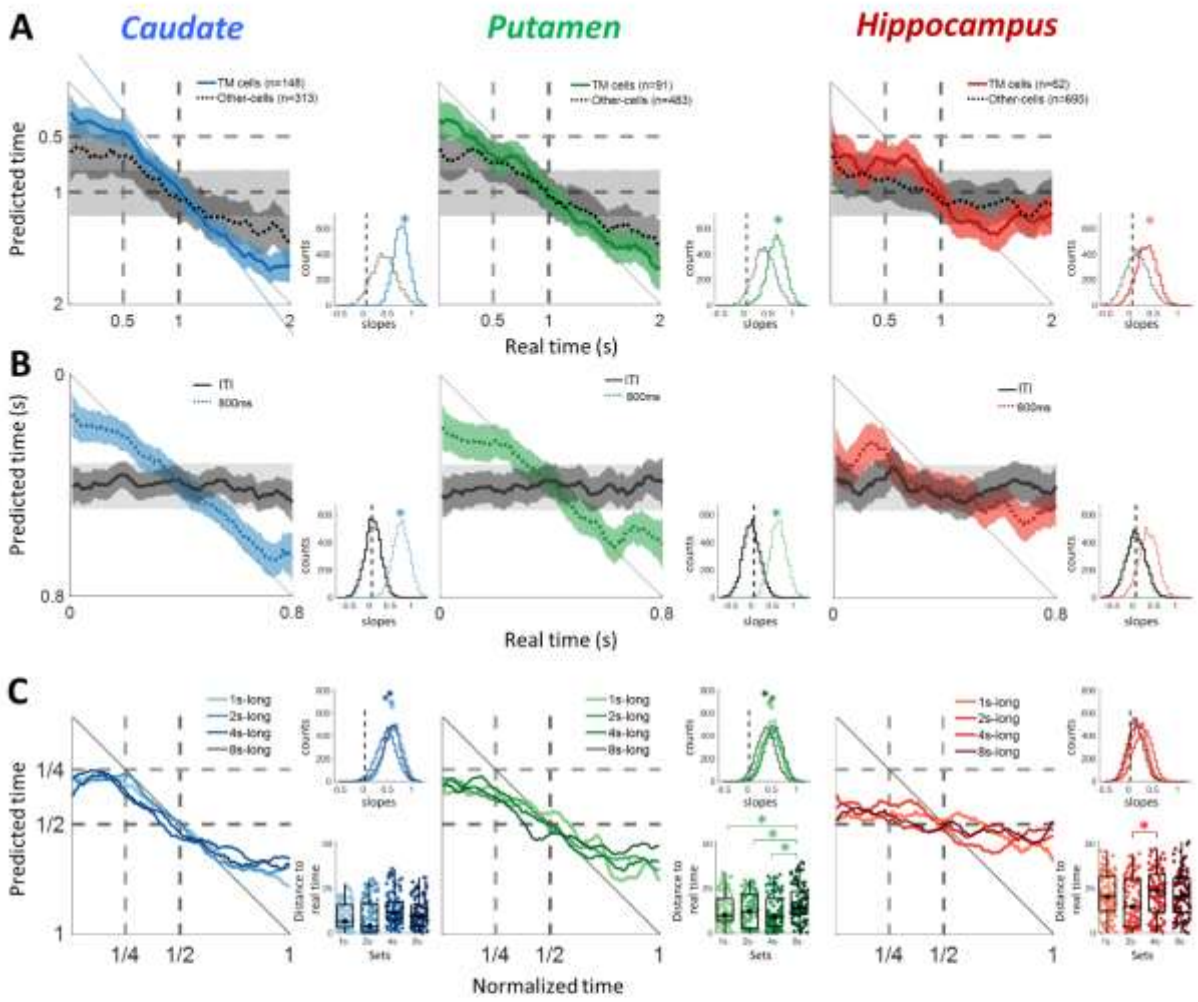

565

566

567 Figure 6

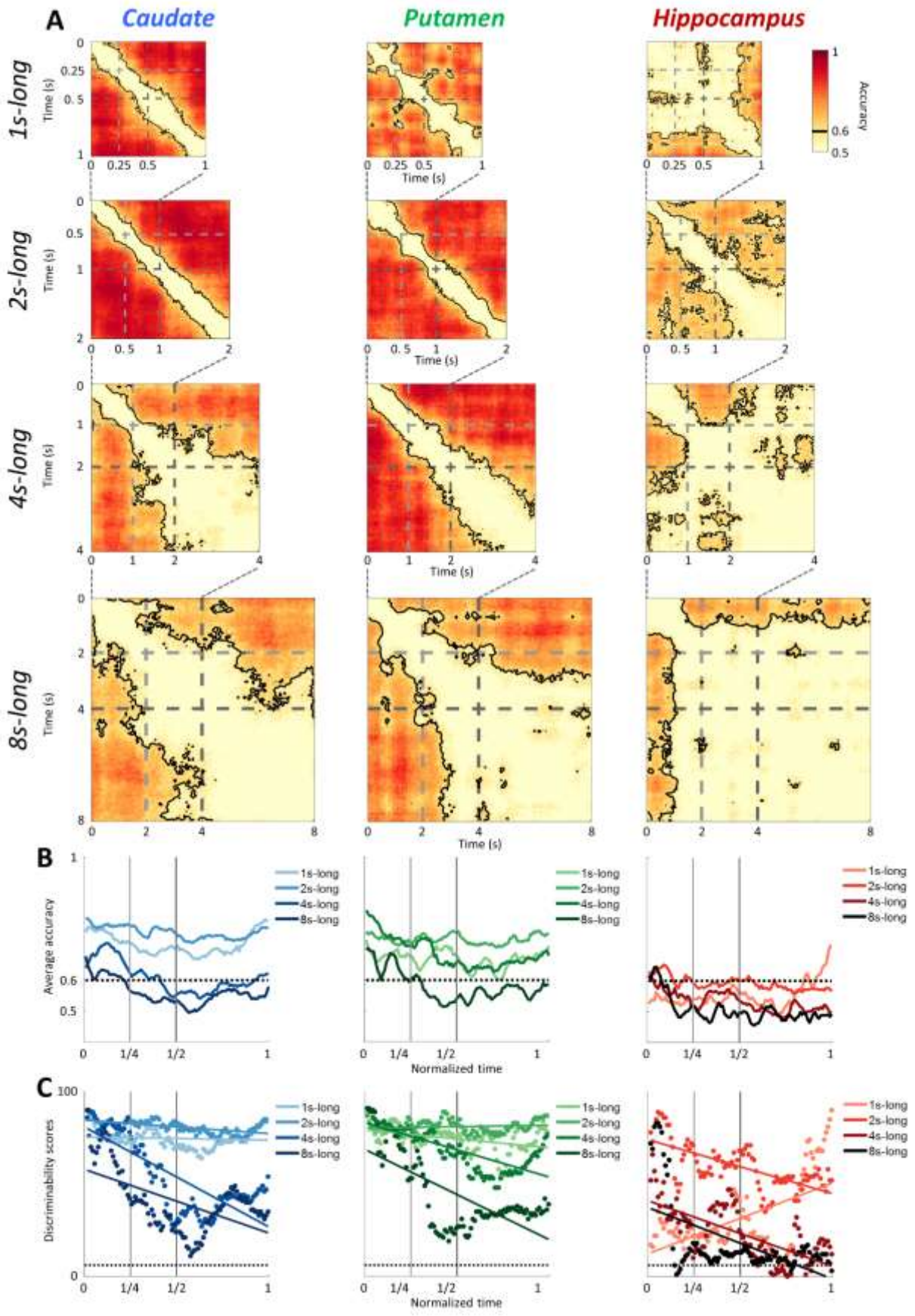

568

569

FIGURE LEGENDS

Figure 1. Ongoing time categorization task and striatal and hippocampal neuronal population.

A. The ongoing time categorization task. A trial started when a white square (cue) was briefly presented on the screen (200ms), marking the beginning of the duration to be timed, and ended when three blue squares (responses targets) appeared at the bottom, left and top of the screen (Figure 1A). Depending on the elapsed time (interval), the monkey used a joystick to move a pointer to the bottom square for short, to the left one for intermediate, or to the top one for long (respectively 0.5, 1 and 2s). Movements performed too early resulted in aborted trials. If the response was correct, the monkey was rewarded with a drop of juice. The inter-trial interval (800ms) started once the monkey moved back the joystick to the centre of the screen. **B. Sets of intervals tested across time-ranges.** Length of the durations at sub-second (0.25-0.5-1s), second (0.5-1-2s), supra-second-1 (1-2-4s) and supra-second-2 (2-4-8s) ranges. **C. Behavioural categorization of intervals across sets.** Proportion of correct responses for short, intermediate and long intervals across sets for Monkey#1 (M#1, left panel) and Monkey#2 (M#2, right panel). Effects of time range and intervals were tested with a general-linear mixed-model (GLMM), showing a significant effect of time range ($F(3,74232)=637.35$, $p<0.0001$), interval ($F(2,74232)=762.53$, $p<0.0001$) and interaction ($F(6,74232)=151.53$, $p<0.0001$). **D. Nature of errors for intermediate trials** across sets. The left values indicate underestimations and the right values indicate overestimations. From top to bottom, intermediate trials at sub-second, second, supra-second-1, supra-second-2 ranges. **E. Psychometric curves across ranges.** Probability to respond long (p(long response), y-axis) after short, intermediate and long intervals (x-axis) depending on the time range (coloured lines). Results for Monkey#1 are shown by solid lines and for Monkey#2 by dashed lines. **F. Behavioural Coefficient of Variation.** Coefficient of Variation (CV, y-axis) displayed for short, intermediate and long intervals (x-axis) as a function of time-range (colours) for both monkeys separately. Each dot (circle or square respectively for Monkey#1 and Monkey#2) represents a block of behavioural performance. Averaged CVs and +/-1 standard deviation for both monkeys' performance merged are shown with black diamonds and lines. Colour code is the same as in E. **G. Response time density for each interval across sets.** Response time

normalized to mean motor response (STAR Methods) for Monkey#1 (top row) and Monkey#2 (bottom row). A linear mixed-model (LMM) shows an effect of time range ($F(3,61185)=1.2962e3$, $p<0.0001$), interval ($F(2,61185)=549.9881$; $p<0.0001$), and a significant interaction ($F(6,61185)=700.19$, $p<0.0001$). **H. Recording sites.** Recording sites in both monkeys: blue dots for caudate, green dots for putamen and red dots for hippocampus. Hippocampus coordinates of both monkeys are aligned to the inter-aural, striatal coordinates are aligned to the anterior commissure. **I. Percentage of Time-Modulated cells.** Sets are displayed in rows, brain regions in columns. In each column, the left pie represents the percentage of TM cells obtained during the long interval of the set. The right pie represents the percentage of TM cells obtained for the first second only when it was taken from the long interval.

Figure 2. Time-Modulated single cell examples during the second range set.

From left to right columns, raster histograms of spikes recorded in the caudate, putamen and hippocampus with the superposed average activity (lines). Left panels show the activity during baseline, the cue, and the long interval, aligned at 0, the offset of the cue. The possible short and intermediate intervals are marked by red lines. Right panels show the neural activity aligned to the reward delivery (black line), with -300ms corresponding to movement. All trials, short, intermediate and long, are displayed, respectively indicated with light grey, dark grey and black. Per each cell, we indicate its bit/spike score and its p-value in parenthesis. See also Figures S1 & S2.

Figure 3. Population changes through time across regions at set 2s-long.

A. From left to right, neuronal population of TM cells recorded in the caudate (left), putamen (middle), and hippocampus (right). Activity is z-scored. Neurons are sorted as a function of their linear term computed during the stepwise regression analysis. Superposed on the population maps, solid line and dotted lines show average z-score and standard-deviation. Time of expected interval ends are indicated with white vertical lines. **B.** Population activity over time (set 2s-long) projected onto the first two Principal Components for the caudate (left), putamen (middle), and hippocampus (right). Each coordinate is the score of each principal component at time t_1 *to* t_{100}. The time of expected interval ends are indicated for short (S),

intermediate (I) and long (L) intervals. The centroid of the distribution is represented with a cross. **C.** Average speed (y-axis) of the neural trajectories during the 2s-long interval, obtained with the first 11 PCs, from each iteration, with the down-sampling method (*i*=1000) plotted against the average distance to the centroid of the same trajectories (x-axis). **E.** Average speed (y-axis) of the neural trajectories obtained from each iteration (*i*=1000) for each brain region across sets (x-axis). **F.** CV (y-axis) of the neural trajectories obtained from each iteration (*i*=1000) for each brain region across sets. **D.** Distribution of angular positions computed from each iteration (*i*=1000) at each time-point. White circles indicate the angle obtained with the highest probability (best angle) for the 1000 iterations, for each time-point. Time of expected interval ends are indicated with white vertical lines as in A. See also Figure S3.

Figure 4. Non-scalar scalability in caudate between sub-second and second ranges.

A. Neural trajectory of caudate neurons during sets 1s-long (purple) and 2s-long (orange) represented by PC1 (x-axis) and PC2 (y-axis) scores obtained from 20ms-bins. Each dot represents the scores for a time-bin obtained on one of 1000 iterations from the down-sampled data. Solid lines show the averaged trajectory. Circled point, cross and asterisk show respectively the short (1/4), the intermediate (1/2) and long interval. **B.** Hypothesis space to interpret the overall geometry of neural trajectories as a function of rescaling. The distance between neural trajectories across time is plotted according to absolute (in black) and relative sampling (in grey). For absolute sampling, we use all the bins of 1s-long interval and only the first half of 2s-long one. For relative sampling, all time bins of set 1s-long are included but only every odd sample of set 2s-long are included. Plotting distances between neural trajectories according to relative sampling should result in a flat line if the trajectories rescale proportionally (third row, left panel, grey line on the bottom left), or on the contrary as a gradual increase if the trajectories do not rescale proportionally (third row, right panel, grey on the bottom right plot). The inverse relationship can be derived for absolute sampling (Third row, black lines). **C.** Top panel. Distances between trajectories for absolute (black) and relative (grey) sampling computed on each one of the 1000 iterations. Bottom left. Distribution of the slopes obtained for the relative sampling (βr). Bottom right. Distribution of the slopes obtained for the absolute sampling (βa). **D.** Distribution of the PC1 scores (top) and PC2 scores (bottom) from the 1000 iterations for set 2s-long (orange) and set 1s-long (purple) at the final point of

the trajectories (asterisks in A) for a relative comparison, end to end. **E.** Distribution of the PC1 scores (top) and PC2 scores (bottom) from the 1000 iterations for set 2s-long (orange) and set 1s-long (purple) at the final point of the trajectories of set 1s-long (asterisks in A, top row) and the half of the interval of set 2s-long (cross in B, bottom row) for an absolute comparison, 1s interval between ranges.

Figure 5. Population decoding as a function of time.

A. Multiclass decoding during 2s-long interval for the caudate (left), putamen (middle) and hippocampus (right). Decoding of predicted time (y-axis) as a function of real time (x-axis). Decoding performance on TM cells (coloured line) is represented against decoding performance on other cells (dotted black line). Chance value is shown with light grey shade. Possible interval ends are indicated by light grey (short) and dark grey (long) dashed lines. Bottom right panel insets: Slopes distribution obtained from the 5000 decoding outputs for TM cells versus other cells. TM cells slopes distributions were higher than other cells slopes distribution for any region (n=5000, 2-samples T-test, for all regions, T(9998)=68.64 for caudate, T-stat=61.7118 for putamen, T-stat=52.9489 for hippocampus, p<0.0001 for all brain regions). Chance level (95^{th} percentile of the distribution) is represented in dashed lines. Distributions of TM cells slopes were different from chance (p=0, p=0.001 and p=0.049, respectively for caudate, putamen and hippocampus) and are indicated with an asterisk. Other cells slope distribution did not differed from chance level. **B.** Multiclass decoding tested on activity during the ITI (black line) after training on the first 800ms of the interval (coloured line) for the caudate (left), putamen (middle) and hippocampus (right). Decoding of predicted time (y-axis) as a function of real time (x-axis). Bottom right panel. Slopes distribution obtained from the 5000 decoding outputs of first 800ms (coloured dotted line) and baseline activity (black line). Distributions different from chance are indicated with an asterisk. **C.** Decoding across sets after down-sampling the populations for the caudate (left), putamen (middle) and hippocampus (right). Decoding of predicted time (y-axis) as a function of normalized time (x-axis). Possible ends of intervals are indicated by light grey (short) and dark grey (long) on the normalized time axis. Top right panel. Distance from predicted time to real time for each time-point of the decoded interval. Bottom right panel. Slopes distribution obtained from the 5000

692 decoding outputs at each set. Chance level (95th percentile of the distribution) is represented
693 in dashed lines. Distributions different from chance are indicated with an asterisk. See also S4.
694

695 **Figure 6. Time-by-time discrimination.**

696 **A.** Pairwise decoding for the caudate (left), putamen (middle) and hippocampus (right).
697 Results for each set are presented in rows: from top to bottom are sets 1s-long, 2s-long, 4s-
698 long and 8s-long, and displayed in a time-by-time matrix in which each data-point is the
699 discriminability accuracy between t(*x*) and t(*y*). Accuracy scores ranged from 0.5 to 1. Chance
700 level is defined at 0.6. The temporal resolution is the window within the diagonal between
701 black lines (chance level). Times for possible intervals to end are shown by light grey (short)
702 and dark grey (intermediate) dashed vertical and horizontal lines. **B.** Average accuracy over
703 time for the caudate (left), putamen (middle) and hippocampus (right) across ranges (coloured
704 lines). Times for possible intervals to end are indicated by solid vertical lines, light grey for
705 short and dark grey for intermediate. Dotted line represents the chance level. **C.**
706 Discriminability scores (dots) across sets for the caudate (left), putamen (middle) and
707 hippocampus (right). Each time on the x-axis (normalized time) is discriminated from n-points
708 on the y-axis within the intervals. Coloured lines show the regressions of the accuracy scores
709 by normalized time. Times for possible intervals to end are indicated by solid vertical lines,
710 light grey for short and dark grey for intermediate. Dotted line indicates the chance level (=.6).
711 See also S5.

712

713

714

715

716

717

718

719

STAR METHODS.

RESSOURCE AVAILABILITY

Lead contact.

Further information and requests for resources should be directed to and will be fulfilled by the lead contact, Sylvia Wirth (sylvia.wirth@isc.cnrs.fr).

Material Availability.

This study did not generate new unique reagents.

Data and code availability.

All data and original code has been deposited at [*link will be made public upon acceptance*] and is publicly available as of the date of publication. DOIs are listed in the key resources table.

Any additional information required to reanalyse the data reported in this paper is available from the lead contact upon request.

EXPERIMENTAL MODEL AND SUBJECT DETAILS

Animals and surgical protocols.

Two naïve adult female rhesus macaques (Monkey#1, 6.5 kg, and Monkey#2, 7kg, both 5 years old at the beginning of the experiments) were housed in the same group of four females. Surgical, behavioural and experimental procedures were authorized by the ethical comity of animal experimentation N°42 and by the French minister of research and innovation under the number APAFIS#13212-20180125104191. Under general anaesthesia, the animals were implanted with a rectangular nylon chamber (21x15) on the right hemisphere allowing simultaneous access to the striatum and the hippocampus (coordinates of the centre of the chamber relative to inter-aural line, for Monkey#1, AP: +14, ML: +11; for Monkey#2, AP: -15, ML: +10; Figure 1H). The anaesthesia for the surgery was induced by Zoletil (Tiletamine-Zolazepam, Virbac©, 5mg/kg) and maintained by isoflurane (Belamont, 1–2%). Pain during and after surgery was controlled by buprenorphine (Temgesic0.3mg/ml, 0.01mg/kg), and prophylactic antibiotics were administered. A head-post was also implanted and covered by

bone cement (Palacos©). The surgical procedures conformed to European and National Institutes of Health Guidelines for the Care and Use of Laboratory Animals.

METHOD DETAILS

Behavioural training and task design.

Before experiments took place in the laboratory, animals were trained to enter a primate seating chair via positive reinforcement through clicker training and gradually habituated to be brought outside the animal facility to the lab. Animals were taught to touch an object to obtain a reward in their cage, then, they were brought to the lab, where they were also rewarded to touch and manipulate a joystick. After this initial period, proper task training followed. The task was programmed using Presentation (Neurobehavioral systems), which controlled reward deliveries conditioned to the movements of the joystick (Sakae Tsushin Kogyo, L.T.D.) depending on task contingencies. Monkeys were seated at a distance of 55cm from a 1024x768 screen with a refreshing rate of 60Hz. The experimental chair allowed reaching the joystick placed in front of the animal. Both monkeys preferred to use their right hand to manipulate the joystick. We first trained the two macaques to associate the movements of the joystick to a pointer on the screen. Following the presentation of a brief white square (200ms interval start cue), if the animal moved the pointer via the joystick to a target (a blue square), it was rewarded by a small amount of diluted juice delivered close to its mouth. The square (150x150 pixels) was randomly positioned at the top, bottom or left of the screen on every trial. Once the monkey learned the motor movements to reach targets in the three positions, three intervals were progressively inserted between the cue and the target. The screen remained dark during these intervals. We first trained the monkeys to discriminate the durations at the second-range for months (2 blocks a day, for circa 12 weeks), hereby resulting in an overtraining at this specific time-range that could explain better performances. On each trial, the monkey waited for .5, 1 or 2s (respectively short, intermediate and long trials for the set 2s-long) between the white square offset (start cue) and the targets' appearance, without moving the joystick. In an initial training phase, the monkey was presented with an interval duration individually, and learned to move the joystick to its respective target. Then, to induce the time-based decision, we interleaved trials with two intervals during a block, and at the end of each interval, only two targets appeared at the screen, bottom and top). The monkey had to learn which (top or bottom) target was correct

as a function of interval duration. Then, when the monkey correctly categorized short and long intervals, it faced short-intermediate or intermediate-long on different blocks. This latter training phase was longer then for the first one. Finally, trials with all 3 intervals were interleaved within a block. Therefore, even though the three durations were presented with equal probability during the recording sessions, it is interesting to note that, despite the fact that monkeys were exposed more frequently to the intermediate interval, that interval remained the most challenging duration to categorize (Figure 1C). Monkeys received three possible rewards, lasting 100, 200 or 400ms for Monkey#1 and 75, 150 or 300ms for Monkey#2. Reward sizes were kept the same across sets, and were intermixed with any possible interval length. If the monkey moved the joystick before the end of the interval, the trial was aborted without reward given. The inter-trial interval started when the monkey reset the joystick position.

Retiming sets.

When the monkeys reached 80% of correct responses at categorizing durations at set 2s-long, we tested them on different sets. First, for several blocks, the monkeys started with set 2s-long, and then the durations were halved: long became 1s, intermediate 0.5 and short .25s (set 1s-long, or sub-second range). Then, we tested the monkeys on set 4s-long (supra-second range-1) following the same procedure. Monkeys started a block with set 2s-long and after circa 100 trials, the durations were multiplied by 2: long became 4s, intermediate 2 and short 1s. Once monkeys adapted to this new retiming condition (retiming long), it had to discriminate even longer durations following the same rule: once they performed enough trials at set 4s-long, durations were multiplied by 2 once more, reaching 8s, 4s, and 2s (set 8s-long or supra-second range-2). Once monkeys learned the retiming rules, we tested them on the same durations, but starting from set 8s-long, then retiming to 4s- and finally to 2s-long. We recorded from both monkeys while they performed one block of one set followed by a second set. By employing this approach, the monkeys were not excessively trained in any of the retiming sets. Consequently, the training history cannot account for the variations in performance observed among these sets. To summarize, blocks could start with 2s-long followed by 1s-long, or with 2s-long followed by set 4s-long and set 8s-long (Figure 1B). Therefore, the task design led to the limitation that all cells were not recorded for all sets, and

thus we recorded from many more neurons in set 2s-long, as this was the reference set. For Monkey#1, a few sessions consisted of set 2s-long only.

Electrophysiological recordings.

Neural activity was recorded using the AlphaLab SNR version 2.0.4 (AlphaOmega©). Single-unit responses were recorded using a 16-channel laminar probe with 300-µm inter-electrode spacing (V-probe, Plexon Inc.; LMA Microprobes). Two such electrodes were inserted simultaneously on every recording session, alternatively in the caudate and the hippocampus, or the putamen and the hippocampus. Cells were isolated offline using a semi-automatic method and checked manually using Offline Sorter (Version 3 and 4; Plexon Inc.) We recorded 615 neurons in the caudate (151 in Monkey#1, 464 in Monkey#2), 736 in the putamen (177 in Monkey#1, 559 in Monkey#2), and 929 in the hippocampus (291 in monkey 1, 638 in monkey 2). Among caudate neurons, 196, 461, 204, 170 cells were recorded respectively during sets 1s-, 2s-, 4s- and 8s-long. Following the same order, 199, 574, 333, 239 neurons were recorded in the putamen, and 348, 759, 340, 203 neurons in the hippocampus. We recorded from many more neurons in set 2s-long, as this was the reference set. For Monkey#1, a few sessions consisted of set 2s-long only.

QUANTIFICATION AND STATISTICAL ANALYSIS

All analysis was done using custom written scripts in MALTAB R2018b (The MathWorks Inc., Natick, Massachusetts).

Behavioural analysis.

To ensure comparability of behavioural and neural activity across ranges, we only included sessions that were above a behavioural criterion. This criterion was determined using a performance threshold (proportion of correct responses), calculated by subtracting one standard deviation from the average performance across all recorded sessions. To take into account variability between time ranges, the threshold was adjusted to the behavioural performances within a time range. This conservative approach ensured that the data analysis was conducted on sessions in which the animal was truly engaged in the task. For Monkey#1, performance thresholds, expressed in proportion of correct responses, were set at 0.74, 0.72,

0.60, and 0.58 for the sub-second, second, supra-second-1, and supra-second-2 ranges, respectively. For Monkey#2, the thresholds were 0.65, 0.73, 0.59, and 0.44, following the same order. The analysis included 54, 151, 77, and 54 blocks (with 1 to 3 sets per recording session) for Monkey#1, totalling 41,598 trials. For Monkey#2, the analysis covered 55, 118, 64, and 51 blocks for the sub-second, second, supra-second-1, and supra-second-2 ranges, respectively, amounting to 32,588 trials in total. At the beginning of each set, we systematically excluded the 10 first trials from all the analyses to remove a potential effect of the behavioural adjustment between ranges, as there was no indication of a switch in sets, except through previously correct response becoming incorrect. To take into account the trial-by-trial variability, ssubsequent behavioural analysis was carried out on a trial-by-trial basis, leading to a high degree of freedom. Next, we used a General-Linear Mixed-Model (GLMM) model to identify whether the time range (*i.e.* the Time Range) or the interval durations (short, inter, long, *i.e.* Interval), monkey's identity (i.e. Monkey ID) and testing day (i.e. Block) influenced discriminability:

$$\text{Response} \sim \text{Interval} * \text{Time Range} + (1|\text{Monkey ID}) + (\text{Monkey ID}|\text{Block})$$

where 'Interval' and 'Time Range' were categorical fixed factors, and the block and monkey's identity were random factors, respectively numerical and categorical. This method avoids treating trial sub-samples as independent values, as we also incorporated the 'Block' factor. The accuracy followed a binomial distribution, 1 or 0, for respectively correct and error trials.

To determine the nature of error for intermediate trials, we performed a GLM on the response of incorrect trials (*i.e.* Type of error) as a function of the time range of the set (Time Range) and the testing day (Block).

$$\text{Type of error} \sim \text{Time Range} + (1|\text{Monkey ID}) + (\text{Monkey ID}|\text{Block})$$

with Time Range as main factor and the type of error as explained variable (with 0 for short and 1 for long). Monkey ID and Block were defined as random factors. Type of errors were significantly influenced by the time range.

To examine whether the probability to respond 'long' across different ranges followed a scalar pattern, we constructed psychometric curves. Note that there were only three intervals to categorize compared to bisection tasks for which classic psychometric curves are constructed with more durations[68 69], preventing us computing classic metrics to test scalar property of

behavioural timing[70]. Hence, for each range we computed only three values: the probability of responding 'long' after a short interval, after an intermediate interval, and after a long interval. These individual "psychometric curves" were generated for each monkey. We subsequently applied a logarithmic model to each curve:

$$Y = a + b * \log(x)$$

In this equation, "a" and "b" represented free parameters, while "x" denoted the empirical data gathered on the probability of responding "long" after short, intermediate, or long trials. We performed this analysis for each range, considering each block separately and averaging responses per block. Subsequently, for each monkey individually, we tested the effect of time range on the "b" parameters using a 1-way ANOVA.

For the behavioural Coefficient of Variation (CV), we calculated a CV for short, intermediate, and long trials within each set of every block, separately for each monkey. The CV was computed as follows:

$$CV = \mu / \sigma$$

where μ represents the average of correct categorizations, and σ denotes the standard deviation. These calculations were based on distributions with values of 0 and 1, corresponding to error trials and correct trials, respectively. Subsequently, we examined the CV variations across trial types and ranges using the following GLMM:

$$CV \sim Interval * Time\ Range + (1|Monkey\ ID) + (Monkey\ ID|Block)$$

In this equation, Interval, Time Range, Monkey ID, and Block are the same factors as in the previous models. The key distinction is that in this context, CV serves as a block-by-block measure, whereas in the other models, Response and Type of Errors are evaluated on a trial-by-trial basis. The main effects were then tested using a 2-way ANOVA on the models.

We tested another trial-by-trial model on normalized response latencies, after selecting correct trials only:

$$Response\ latency \sim Interval*Time\ Range + (1|Monkey\ ID) + (Monkey\ ID|Block)$$

Response latencies calculation and normalization. We calculated response latencies for each interval (short, intermediate, long) by measuring the time between the target onset and the

action completion. However, to account for differences in motor production times associated with different required responses (bottom, left, top), we normalized these response times by the ones obtained in a "motor-control task". After each block, monkeys were tested on a "motor-control task", where no delay was inserted between cue offset and targets onset. Only one target was presented at the time, for a total of ~70 trials per block. The monkey had to move for the presented target, getting an immediate reward. Latency measures in this task revealed differences in the response times among the three motor productions (bottom-short, left-intermediate, top-long). Specifically, left movements were significantly faster (1-way ANOVA, $F(2,22026)=89.3$, $p<0.0001$) than bottom and top movements, while latencies for bottom and top responses did not differ from each other. This suggested our monkeys were more proficient in performing a left joystick movement compared to top or bottom. To standardize the response times, we subtracted the average latencies obtained from the "motor-control task" for each direction from the corresponding latencies obtained at each trial during the categorization task. This normalization gives us a result for which responses latencies below 0 reflected anticipation of the end of the interval, as the response latency was below the time needed for action selection/execution when the monkey was presented one target at a time with no delay.

Information content computation.

To define time-modulated cells, we computed a "Time" Information Content (IC) and tested whether the IC_{real} obtained on the actual data was above that of an IC obtained by chance. The time IC_{real} reflects the information carried by a spike as a function of a time-bin weighted against all time-bins, and when tested against chance, allows determining whether actual pattern of firing rate as a function of time differs from chance. Importantly, the aim here is to test the hypothesis that an IC above chance reflects a temporal organization across time different from the one that could be just random. We calculated the IC_{real} for each cell following the next formula:

$$IC = \sum \lambda(x) * \log(\lambda(x)/\lambda)$$

where $\lambda(x)$ is the firing rate of the neuron at time t, λ is the overall firing rate, from t_1 to t_{100}. Due to the formula's sensitivity to the number of bins, the IC value decreases when the number of time bins increases, as the firing rate within each time bin depends on the total

count of time bins. Therefore, to ensure consistency in comparisons across different time ranges, we opted to divide the longer interval within each set into 100 bins. The size of the bins varied between ranges (*i.e.* 10ms, 20ms, 40ms, and 80ms respectively for sets 1s-, 2s-, 4s- and 8s-long) but the total number of bins did not. Next, we shuffled the spikes within the interval 1000 times, and, at each time, we calculated an IC_{fake} on the shuffled data. With these 1000 permutations, we computed a distribution of 1000 IC_{fake}. We defined time-modulated cells as neurons that had an IC_{real} superior to 95% of the IC_{fake} obtained by chance (*p*-value calculation). Additionally, neurons identified as TM cells at the sub-second and second ranges exhibited robust cross-correlation between the first and second halves of the trials, demonstrating stability of the temporal pattern within the session (data not shown). Non-significant neurons were defined as other cells. This procedure was repeated for all ranges.

To test whether the proportion of TM cells changed if only the first second is considered for all sets, we cropped all correct long trials after 1s and then computed the IC_{real} value for each neuron on this 1s, for all conditions. As the number of bins strongly influence the value of the IC and the permutation test, this cropping method allows a proper control across ranges with an absolute bin size and the comparison across ranges for this analysis is then not sensitive to the length of the interval. Thus, we identified TM cells with IC_{real} significance computed on 100x10ms bins of the first second of the 2s-long (cropping the second half), 4s-long (cropping the next 3s) or 8s-long interval (cropping the next 7s), and compared them to the 100 bins of the 1s-long interval of the sub-second range. We followed the same procedure, as before, shuffling the spikes within trials across the first second for all trials, to calculate the *p*-values within the first second.

In the same way, we identified TM cells on the inter-trial interval (ITI). Neural activity within the ITI was divided into 100x8ms bins and the IC was calculated in this segment. Again, per each neuron, we compared this IC_{real} versus the distribution of IC_{fake} obtained after spike shuffling and obtained a *p*-value.

Definition of the neural pattern of single-cells.

To classify the single cells as ramping or peak neurons, we used a stepwise regression analysis to test whether a linear or a quadratic term best explained the neural activity of each neuron during the interval. We defined a cell as ramping when 1) the linear term explained best the

firing rate throughout the interval and 2) the R^2 of the fitted model explained at least 66% of the variance. For cells that did not reach those criteria, we tested whether their neural activity exhibited a peak, defined as an increase of 80% above their maximal activity followed by a decrease of at least 15%. If they did, and that only one peak was found in the interval, they were classified as 1-peak neurons. If they did, and several peaks were found in the interval, they were classified as n-peaks neurons. The latter cells exhibited one or more "time fields" and made up the majority of the population in all regions (Figure S1A). The "time field" size was defined, in seconds, as the width of the peak measured at half of its prominence. For peak time analysis (Figure S1E-G-H), we only took the highest peak time of the n-peaks neurons.

Neuron's selectivity to motor preparation and execution

We tested whether the single cells responses could be associated with the motor responses during the task, by using an ANOVA and post-hoc analysis, on the trial-by-trial activity exhibited during the 300ms of the movement execution. Next, focusing on TM cells recorded during both the 1s-long and 2s-long sets in the caudate (n=87) or the putamen (n=38), and using correct trials, we analysed the last 200ms before target presentation for long (top movement), intermediate (left movement), and short (bottom movement) intervals via a 2-way ANOVA.

Neurons selectivity to epochs of the task.

To identify neurons that were selective for other epochs of the task (cue, target, response and reward), we tested a GLMM to identify if 1) neurons were responsive to each task epoch in comparison to the baseline, and 2) if there was a difference in that epoch as a function of short, intermediate and long trials (Interval). The GLMM was computed on each neuron's firing rate trial-by-trial at the second range following the formula:

$$\text{Firing Rate} \sim \text{Task Epoch} * \text{Interval} + (1|\text{Trial})$$

where Firing Rate is expressed in spikes/second, Task Epoch is a categorical variable for which the modalities are the baseline (inter-trial interval), and separately, either the cue display (200ms), the targets displayed (400ms), the movement preceding reward (-400ms before reward delivery) and reward delivery (200ms). Thus, GLMM were computed separately for each feature. Interval identity is a categorical variable, either "short", "intermediate" or "long". Trial is a random factor. This model allows to identify the baseline activity different

from another task epoch per each neuron. If the task epoch was significantly different from the baseline, then we tested if there was a difference as a function of interval identity. We defined neurons as selective for one interval when its activity for that interval was significantly different from the other two, and these other two intervals did not differ from each other.

Down-sampling methods.

To address the imbalance in sample sizes across various regions and time ranges, we consistently applied down-sampling techniques in all our population analyses. This involved computing measures (PCA) or cross-validating analysis (linear-regression-based decoding and SVM-based decoding) on subsamples drawn over multiple iterations. During each iteration, we randomly selected a subset of neurons (N), with N being determined by the smallest TM cell population size (31 for putamen and hippocampus within the sub-second range). For PCA and linear regression-based decoding, a subset of 28 neurons (leaving 3 out) was drawn at each of 1000 iterations for each brain region and time range. In the case of SVM-based decoding, a subset of 30 neurons (leaving 1 out) was randomly drawn for 10 iterations for each brain region and time range. By adopting this approach, results across regions and time ranges were minimally affected by variation in neural population size.

Principal Component Analysis.

We computed Principal Component Analysis (PCA) for each set and each brain region on correct long trials within the set. For each neuron, we used the raw activity averaged across trials at each time-bin. Each neuron was defined as a variable and each time-bin was defined as an observation. We performed PCA with the down-sampling method, conducting 1000 measures (as described above) on randomly selected sub-populations of 28 neurons for each region within each time range. On each iteration, we determined the number of components needed to capture at least 50% of the variance (Figure S3A), as measures of speed and distance to centroid are computed based on this number of PCs. Thus, we selected 11 components, which represented the highest number of PCs needed to capture at least 50% of the variance across regions and time ranges (observed in the putamen and the hippocampus for the 8s-long set, see Figure S3A). Our choice of a 50% threshold differs notably from the conventional approach[66 22 6], mainly because we performed PCA on raw spiking activity. However, we determined that this equaled 80% of the variance explained when PCs were

computed on smoothed data. Next, the speed (Figure 3C-D) was calculated on each iteration as the Euclidean distance between the PC scores of two consecutive time-bins. Importantly, to compute speed (and other measures below), we employed an absolute binning approach using 20ms bins across all ranges, as it is essential to maintain a consistent binning method to measure true differences from time to time. Consequently, the number of time-bins increased significantly as the time range expanded: from 50 time-bins in the sub-second range to 100, 200, and 400 in the second range, supra-second range-1, and supra-second range-2, respectively. The Coefficient of Variation (CV= μ / σ, Figure 3E) was computed by taking the average speed (μ) on each iteration and dividing it by the standard deviation (σ). Following a similar rationale, we determined the centroid as the point equidistant from the scores at each time-bin. We then computed the average distance to centroid on each iteration, as a mean to compare across time ranges, as the number of observations varied between ranges. The distances to the centroids were expressed in Euclidean distances with the following formula:

$$D(x,c) = (x_{i,j,k}-c_{i,j,k}) * (x_{i,j,k}-c_{i,j,k})'$$

Where x is the state of the population at time *t* and c is the centroid of the distribution X. i, j, and k are the coordinates in the 3-dimensional state.

Separately, we determined the angular position of the scores' coordinates at each time-bin (ranging from 1 to 100, normalized time) by calculating the angle formed between: 1) the scores at the first time-bin, 2) the scores at the current time-bin's position (from 1 to 100), and 3) the centroid of the trajectories. This equals to determine the angular progression of the hands of a clock ranging from the first to the last bin. For this analysis, as for the IC calculus, we binned the intervals into the same number of time-bins (*i.g.* 100) to prevent an imbalance in the number of observations for across range comparisons. The angular calculation was performed using the first 3 principal components in a trigonometric space using normalized bins. To this end, the time-space was normalized such that angle 1 corresponded to time 1 and angle 360 corresponded to 1, 2, 4 or 8s depending on the time range. For each time-bin, we obtained a distribution of 1000 angles, obtained from each iteration (see the section Down-sampling methods). We then examined whether there was a consistent progression in neural trajectory over time. To accomplish this, we identified the most frequently occurring angle (referred to as the best angle) from the 1000 iterations at each time-bin (depicted as a white circle in Figure 3F and Figure S3C-E-G, bottom rows). Subsequently, we calculated the

difference between the best angles of two consecutive time-bins for each brain region and range. Finally, we conducted a 2-way ANOVA on these angle differences, with brain region and time range serving as factors.

PCA analysis for rescaling of neural trajectory

For this analysis, we used exclusively the 87 neurons that were recorded across the sub-second and second time ranges, and identified as TM cells in at least one of the time ranges. We performed a PCA on the concatenated rate matrices from the two time ranges using an absolute binning (20ms bins) across time ranges (50 bins for set 1s-long, and 100 bins for 2s-long). The rows for the input matrix corresponded to the firing rate of 87 caudate neurons binned in 20ms. The columns of the input matrix for the PCA consisted of the time-bins of the interval for the two time ranges as follows: the firing rates for each of the 50 time-bins of the 1s-long interval and the firing rate of each of the 100 time-bins of the 2s-long interval.

To compute statistics, we used a bootstrap method in which we drew 30 trials on each of 1000 iterations to compute the PCs on the concatenated matrix. We first extracted the eigenvectors on the entire population, and then projected the data for 15 trials taken randomly from each set at each iteration. To consider the overall geometry of neural trajectories, the distance between neural trajectories across time between 20ms samples of 1s-long and 2s-long conditions was plot according to absolute (1 to 1) and relative sampling (1 to every other one). The slope of the regression of the distances as a function of time was interpreted according to the hypothesis space depicted in Figure 4B.

Multi-class decoding using linear regression.

To predict time based on neural activity, we used a linear regression model to decode time. First, to compare the temporal prediction from TM cells and other cells, we trained the model on the neural activity of the two populations separately. Training phase was computed on the 2s-long interval, during 15 correct long trials and the temporal prediction was tested on 5 separate correct trials. We would like to stress out that the time prediction is based on neural data collected for correct long trials, therefore prediction values cannot be directly linked to the behavioural accuracy, which used both error and correct trials, and hence have to be interpreted differently. Neural activity was cut into 100 bins, of 20ms, and smoothed on +/- 4 bins trial-by-trial. Then, the model was tested on five different correct long trials. The analysis

was cross-validated 1000 times. Per each iteration, we obtained a decoding output y = β0 + β1 * X. In the equation, ***X*** is the matrix of neurons (rows) and time (columns) which represents the real-time activity, ***y*** is the vector which contains predicted time at each one of the 100 time-bins, and ***β1*** is a vector containing the weight of each neuron. As we tested the model on 5 correct trials and cross-validated it 1000 times, we obtained 5000 decoding outputs per each brain region and each population. For each of these 5000 outputs, we calculated the slope of the predicted time (**y**). We get a α_{real} distribution of 5000 slopes of decoding for both populations, TM cells and other cells, for each brain region at set 2s-long. To define our chance-level, we performed the same decoding analysis after shuffling the time-labels on tested and trained trials. Thus, we also obtained a distribution of slopes $\alpha_{shuffle}$ calculated on shuffle data. Decoding above chance was define by $1 - (\sum \beta_{1\,real} > P95(\beta_{1\,shuffle}) / 5000)$. Because our model was trained on neural activity during the timed interval, predictions can only be obtained within the time window and cannot extrapolate beyond the boundaries for under or over-estimations. This approach is therefore solely suitable for assessing the general prediction capability of the entire population within the specified time window. We used the same method to test if the neural activity during the ITI could be decoded from the activity of the first 800ms of the interval (Figure 5B). This time, we trained our model on the first 800ms of 15 trials of 2s-long conditions defined as correct. The cropped interval was cut into 100 bins of 8ms and smoothed on +/-4 bins. The model was then tested on 1) the first 800ms activity of the long interval during 5 different trials and 2) on 5 inter-trials intervals (ITI). Then, we tested the temporal predictability of TM cells identified as such during the ITI, by training and testing the activity on 15 and 5 ITI respectively. For this analysis, the ITI was cut into 100 bins of 8ms and smoothed on +/-4 bins trial-by-trial. In all cases, decoding above chance was tested using the same method to compute the slopes and calculate the *p*-values as before. Finally, to test the performance of decoding across sets, we used the same method, with the exception that, at each iteration, we down-sampled our neural population to 28 neurons. This makes comparisons between sets and brain regions possible. For each set, we took the longest interval of the set, and parsed it into 100 bins: resulting in bin size of 10, 20, 40 and 80ms; as for the PCA angular position calculus. Again, this allowed to keep a constant number of observations across sets to facilitate cross ranges comparisons. For each set, the activity was smoothed on +/-4 bins trial-by-trial. As before, we computed, per each set and each brain region, the distribution of the slopes of decoding outputs on real and shuffled data to test the

temporal predictability versus chance. In addition, we also tested the distances of predicted time to real time to compare brain regions between each other and sets. We averaged our 5000 decoding output to get 1 vector of predicted time. At each time-point, we calculated the distance from predicted time to real time, and then compared the brain regions and sets using 2-way ANOVAs.

Pairwise analysis using Support Vector Machine, and measures derived from decoding accuracy.

To quantify the difference between two time-points t_n and tm within an interval, we used a support vector machine (SVM)-based decoding analysis. At time t_n and t_m, the neural state of the population is given by the activity of n neurons. Unlike the linear-regression-based decoding, which evaluated overall prediction, this pairwise decoding technique offers the advantage of assessing time-by-time discriminability, providing a more precise metric. to compare the activity between brain region and sets, we down-sampled our populations to 30 neurons this time, as neuronal shuffling was also supported by different trial selections across iterations. For each set, we binned the activity of correct long trials into 100 bins, sizing and smoothing them as we did for multiclass decoding across sets. Then, we extracted the 3 first components of the neural state at t_n and t_m using PCA on trial-by-trial basis. After dimensionality reduction, the neural state at t_n and t_m are given by 3 coordinates instead of n (*n*=30). Then, we trained a SVM classifier on the 3 PCs of 10 trials from t_n and 10 trials from t_m, and tested it on the PCs obtained from 10 different trials of t_n and 10 others of t_m. The SVM classifier returns an accuracy value between 0.5 and 1: 1 reflects the absolute certainty to classify each time-point (t_n and t_m) correctly, and 0.5 reflects the chance level to distinguish t_n and t_m. Each pair of time-bins, from t_1 to t_{100}, was tested versus each other. We did this analysis for 10 iterations, and represented the averaged outcomes of SVM classifier in a time-by-time matrix, averaging the output of the 10 iterations. To test the temporal accuracy between brain regions and time range, we tested the bottom half along the diagonal of the matrix's accuracies between time range and brain regions using a 2-way ANOVA. Next, we computed the exact same analysis after shuffling the labels on training and test trials. The 95th percentile of the overall distribution of accuracy obtained from shuffled decoding was 0.55. We used a conservative chance level at 0.6. Next, for each time-bin, for each interval, we computed the accuracy score from t_1 to t_{100}.

Discriminability Score. Discriminability score of t_n was defined by the number of time-bins decoded above chance from t_n. Its value ranged from 0 to 99, with 0 indicating that no other time-bin differs from t_n and 99 indicates that all other time-bins of the interval are different from t_n. Then, we calculated the chance level for the number of other time-bins differing from another time-point, with matrices obtained after shuffling the labels, from each region and at all time ranges, and the matrices obtained from each iteration (*i*=10). Per each one of these matrices, we computed the accuracy score of each time-bin. Chance level was defined as the mode of this distribution of 12,000 values.

To compare discrimination per brain region and time range, we regressed the mean discriminability scores as a function of time to test whether they increased or decreased in the interval. an absence of significant linear regression is hence indicative of a constant accuracy within the interval.

Temporal Resolution. To compute the temporal resolution of each brain region across sets, we calculated at each time-bin t_i the distance t_i to t_j, where t_j is the closest time-bin to t_i successfully discriminated from it (above 0.6). To do so, considering the diagonal of our matrices and for each t_i, we identified the distance to the closest time-point decoded above chance at the upper half and the lower half of the matrix, and then averaged these to get the width of the decoding. This distance represents the size of the time window within which neural activity around t_i is too similar to be discriminated from t_i.

To test temporal discriminability in the first second of the intervals across ranges, we used only the first second of the activity of TM cells (cropping off longer intervals). We computed the same decoding analysis, down-sampling our neuronal populations to 18 neurons for each brain region at each time range, except for the caudate at set 8s-long where we had 9 TM cells only. To test whether time was discriminated successfully within one second as a function of time-range, we computed a 2-way ANOVA on the bottom half along the diagonal of the output matrices.

Breaking points. The breaking points in the linearity of the consecutive measures of temporal resolution were identified with the *ischange* MatLab function.

REFERENCES

1. Shikano, Y., Ikegaya, Y. & Sasaki, T. (2021). Minute-encoding neurons in hippocampal-striatal circuits. *Curr. Biol.* **31**, 1438-1449.e6.

2. Tallot, L. & Doyère, V. (2020). Neural encoding of time in the animal brain. *Neurosci. Biobehav. Rev.* **115**, 146–163.

3. Pilkiw, M. & Takehara-Nishiuchi, K. (2018). Neural representations of time-linked memory. *Neurobiol. Learn. Mem.* **153**, 57–70.

4. Shimbo, A., Izawa, E. I. & Fujisawa, S. (2021). Scalable representation of time in the hippocampus. *Sci. Adv.* **7**.

5. Zhou, S., Masmanidis, S. C. & Buonomano, D. V. (2020). Neural Sequences as an Optimal Dynamical Regime for the Readout of Time. *Neuron* **108**, 651-658.e5.

6. Wang, J., Narain, D., Hosseini, E. A. & Jazayeri, M. (2018). Flexible timing by temporal scaling of cortical responses. *Nat. Neurosci.* **21**, 102–112.

7. Mello, G. B. M., Soares, S. & Paton, J. J. (2015).A scalable population code for time in the striatum. *Curr. Biol.* **25**, 1113–1122.

8. Sohn, H., Narain, D., Meirhaeghe, N. & Jazayeri, M. (2019). Bayesian Computation through Cortical Latent Dynamics. *Neuron* **103**, 934-947.e5.

9. Mendoza, G., Méndez, J. C., Pérez, O., Prado, L. & Merchant, H. (2018). Neural basis for categorical boundaries in the primate pre-SMA during relative categorization of time intervals. *Nat. Commun.* **9**.

10. Gouvêa, T. S., Monteiro, T., Motiwala, A., Soares, S., Machens, C. & Paton, J. J. (2015). Striatal dynamics explain duration judgments. *Elife* **4**, 1–14.

11. Skaggs, W. E., McNaughton, B. L. & Gothard, K. M. (1992). An Information-Theoretic Approach to Deciphering the Hippocampal Code. *Adv. Neural Inf. Process. Syst. 5* 1030–1038.

12. Zhou, S. & Buonomano, D. V. (2022). Neural population clocks: Encoding time in

dynamic patterns of neural activity. *Behav. Neurosci.* doi:10.1037/bne0000515.

13. Sarno, S., De Lafuente, V., Romo, R. & Parga, N. (2017). Dopamine reward prediction error signal codes the temporal evaluation of a perceptual decision report. *Proc. Natl. Acad. Sci. U. S. A.* **114**, E10494–E10503.

14. Tiganj, Z., Jung, M. W., Kim, J. & Howard, M. W. (2017). Sequential firing codes for time in rodent medial prefrontal cortex. *Cereb. Cortex* **27**, 5663–5671.

15. Kraus, B. J., Robinson, R. J., White, J. A., Eichenbaum, H. & Hasselmo, M. E. (2013). Hippocampal 'Time Cells': Time versus Path Integration. *Neuron* **78**, 1090–1101.

16. Haber, S. N. (2016). Corticostriatal circuitry. *Dialogues Clin. Neurosci.* **18**, 7–21.

17. Worbe, Y. Baup, N., Grabli, D., Chaigneau, M., Mounayar, S., McCair, K., Féger, J. & Tremblay, L. (2009). Behavioral and movement disorders induced by local inhibitory dysfunction in primate striatum. *Cereb. Cortex* **19**, 1844–1856.

18. Gerardin, E., Pochon, J.-B., Poline, J.-B., Tremblay, L., Van de Moortele, P.-F., Levy, R., Dubois, B., Le Bihan, D. & Lehéricy, S. (2004). Distinct striatal regions support movement selection, preparation and execution. *Neuroreport* **15**, 2327–2331.

19. Buonomano, D. V. & Laje, R. (2010). Population Clocks: Motor Timing with Neural Dynamics. Motor Timing with Neural Dynamics. *Trends Cogn. Sci.* **14**, 520–527.

20. Buonomano, D. V. & Maass, W. (2009). State-dependent computations: Spatiotemporal processing in cortical networks. *Nat. Rev. Neurosci.* **10**, 113–125.

21. Karmarkar, U. R. & Buonomano, D. V. (2007). Timing in the Absence of Clocks: Encoding Time in Neural Network States. *Neuron* **53**, 427–438.

22. Cueva, C. J., Saez, A., Marcos, E., Genovesio, A., Jazayeri, M, Romo, R., Salzman, C. D., Shadlen, M. N. & Fusi, S. (2020). Low-dimensional dynamics for working memory and time encoding. *Proc. Natl. Acad. Sci. U. S. A.* **117**, 23021–23032.

23. Gibbon, J. (1977). Scalar expectancy theory and Weber's law in animal timing. *Psychol. Rev.* **84**, 279–325.

24. Yumoto, N., Lu, X., Henry, T. R., Miyachi, S., Nambu, A., Fukai, T. & Takada, M. (2011). A neural correlate of the processing of multi-second time intervals in primate prefrontal cortex. *PLoS One* **6**, 3–9.

25. Mita, A., Mushiake, H., Shima, K., Matsuzaka, Y. & Tanji, J. (2009). Interval time coding by neurons in the presupplementary and supplementary motor areas. *Nat. Neurosci.* **12**, 502–507.

26. Merritt, D. J., Casasanto, D. & Brannon, E. M. (2010). Do monkeys think in metaphors? Representations of space and time in monkeys and humans. *Cognition* **117**, 191–202.

27. Toso, A., Reinartz, S., Pulecchi, F. & Diamond, M. E. (2021). Time coding in rat dorsolateral striatum. *Neuron* **109**, 3663-3673.e6.

28. Bakhurin, K. I., Goudar, V., Shobe, J. L., Claar, L. D., Buonomano, D. V. & Masmanidis, S. C. (2017). Differential encoding of time by prefrontal and striatal network dynamics. *J. Neurosci.* **37**, 854–870.

29. Naya, Y. & Suzuki, W. A. (2011). Integrating what and when across the primate medial temporal lobe. *Science (80-.).* **333**, 773–776.

30. MacDonald, C. J., Lepage, K. Q., Eden, U. T. & Eichenbaum, H. (2011). Hippocampal 'Time Cells' bridge the gap in memory for discontiguous events. *Neuron* **71**, 737–749.

31. Jazayeri, M. & Shadlen, M. N. (2015). A Neural Mechanism for Sensing and Reproducing a Time Interval. *Curr. Biol.* **25**, 2599–2609.

32. Beiran, M., Meirhaeghe, N., Sohn, H., Jazayeri, M. & Ostojic, S. (2023). Parametric control of flexible timing through low- dimensional neural manifolds. *Neuron* **111**, 1–15.

33. Adler, A., Katabi, S, Finkes, I., Israel, Z., Prut, Y. & Bergman, H. (2012). Temporal convergence of dynamic cell assemblies in the striato-pallidal network. *J. Neurosci.* **32**, 2473–2484.

34. Merchant, H., Zainos, A., Hernández, A., Salinas, E. & Romo, R. (1997). Functional properties of primate putamen neurons during the categorization of tactile stimuli. *J.*

Neurophysiol. **77**, 1132–1154.

35. Korponay, C., Choi, E. Y. & Haber, S. N. (2020). Corticostriatal Projections of Macaque Area 44. *Cereb. Cortex Commun.* **1**, 1–11.

36. Lehéricy, S., Ducros, M., Krainik, A., François, C., Van de Moortele, P.-F., Ugurbil, K. & Kim, D.-S. (2004). 3-D diffusion tensor axonal tracking shows distinct SMA and pre-SMA projections to the human striatum. *Cereb. Cortex* **14**, 1302–1309.

37. Alexander, G. E., DeLong, M. R. & Strick, P. L. (1986). Parallel organization of functionally segregated circuits linking basal ganglia and cortex. *Annu. Rev. Neurosci.* **VOL. 9**, 357–381.

38. Jahanshahi, M., Obeso, I., Rothwell, J. C. & Obeso, J. A. (2015). A fronto-striato-subthalamic-pallidal network for goal-directed and habitual inhibition. *Nat. Rev. Neurosci.* **16**, 719–732.

39. Haber, S. N., Kim, K. S., Mailly, P. & Calzavara, R. (2006). Reward-related cortical inputs define a large striatal region in primates that interface with associative cortical connections, providing a substrate for incentive-based learning. *J. Neurosci.* **26**, 8368–8376.

40. Johnson, E. L., Chang, W. K., Dewar, C. D., Sorensen, D., Lin, J. J., Solbakk, A.-K., Endestad, T., Larsson, P. G., Ivanovic, J., Meling, T. R., Scabini, D. & Knight, R. (2022). Orbitofrontal cortex governs working memory for temporal order. *Curr. Biol.* **32**, R410–R411.

41. Curtis, C. E. & D'Esposito, M. (2003). Persistent activity in the prefrontal cortex during working memory. *Trends Cogn. Sci.* **7**, 415–423.

42. Zhou, J., Jia, C., Montesinos-Cartagena, M., Gardner, M. P. H., Zong, W. & Schoenbaum, G. (2021). Evolving schema representations in orbitofrontal ensembles during learning. *Nature* **590**, 606–611.

43. Wittmann, M. K., Kolling, N., Akaishi, R., Chau, B. K. H., Brown, J. W., Nelissen, N. & Rushworth, M. F. S. (2016). Predictive decision making driven by multiple time-linked reward representations in the anterior cingulate cortex. *Nat. Commun.* **7**, 1–13.

44. Sosa, J. L. R., Buonomano, D. & Izquierdo, A. (2021). The orbitofrontal cortex in temporal cognition. *Behav. Neurosci.* **135**, 154–164.

45. Hare, T. A., Hakimi, S. & Rangel, A. (2014). Activity in dlPFC and its effective connectivity to vmPFC are associated with temporal discounting. *Front. Neurosci.* **8**, 1–15.

46. Grahn, J. A., Parkinson, J. A. & Owen, A. M. (2008). The cognitive functions of the caudate nucleus. *Prog. Neurobiol.* **86**, 141–155.

47. Inase, M., Tokuno, H., Nambu, A., Akazawa, T. & Takada, M. (1999). Corticostriatal and corticosubthalamic input zones from the presupplementary motor area in the macaque monkey: Comparison with the input zones from the supplementary motor area. *Brain Res.* **833**, 191–201.

48. Künzle, H. (1975). Bilateral projections from precentral motor cortex to the putamen and other parts of the basal ganglia. An autoradiographic study in Macaca fascicularis. *Brain Res.* **88**, 195–209.

49. Tremblay, L., Worbe, Y., Thobois, S., Sgambato-Faure, V. & Féger, J. (2015). Selective dysfunction of basal ganglia subterritories: From movement to behavioral disorders. *Mov. Disord.* **30**, 1155–1170.

50. Romo, R., Scarnati, E. & Schultz, W. (1992). Role of primate basal ganglia and frontal cortex in the internal generation of movements. II. Movement-related activity in the anterior striatum. *Exp. Brain Res.* **91**, 385–395.

51. Alexander, G. E. & Crutcher, M. D. (1990). Functional architecture of basal ganglia circuits: neural substrates of parallel processing. *Trends Neurosci.* **13**, 266–271.

52. Martinez, E., Pasquereau, B., Saga, Y., Météreau, É. & Tremblay, L. (2020). The anterior caudate nucleus supports impulsive choices triggered by pramipexole. *Mov. Disord.* **35**, 296–305.

53. Umbach, G., Kantak, P., Jacobs, J., Kahana, M., Pfeiffer, B. E., Sperling, M. & Lega, B. (2020). Time cells in the human hippocampus and entorhinal cortex support episodic memory. *Proc. Natl. Acad. Sci. U. S. A.* **117**, 28463–28474.

54. Itskov, V., Curto, C., Pastalkova, E. & Buzsáki, G. (2011). Cell assembly sequences arising from spike threshold adaptation keep track of time in the hippocampus. *J. Neurosci.* **31**, 2828–2834.

55. Pastalkova, E., Itskov, V., Amarasingham, A. & Buzsáki, G. (2008). Internally Generated Cell Assembly Sequences in the Rat Hippocampus. *Science (80-.).* **321**, 1322–1327.

56. Bright, I. M., Meister, M. L. R., Cruzado, N. A., Tiganj, Z., Buffalo, E. A. & Howard, M. W. (2020). A temporal record of the past with a spectrum of time constants in the monkey entorhinal cortex. *Proc. Natl. Acad. Sci. U. S. A.* **117**, 20274–20283.

57. Reddy, L., Zoefel, B., Possel, J. K., Peters, J., Dijksterhuis, D. E., Poncet, M., van Straaten, E. C. W., Baayen, J. C., Idema, S. & Self, M. W. (2021). Human hippocampal neurons track moments in a sequence of events. *J. Neurosci.* **41**, 674–6725.

58. Mau, W., Sullivan, D. W., Kinsky, N. R., Hasselmo, M. E., Howard, M. W. & Eichenbaum, H. (2018). The Same Hippocampal CA1 Population Simultaneously Codes Temporal Information over Multiple Timescales. *Curr. Biol.* **28**, 1499-1508.e4.

59. Omer, D. B., Las, L. & Ulanovsky, N. Contextual and pure time coding for self and other in the hippocampus. *Nat. Neurosci.* (2022) doi:10.1038/s41593-022-01226-y.

60. Emmons, E. B., De Corte, B. J., Kim, Y., Parker, K. L., Matell, M. S., & Narayanan, N. S. (2017). Rodent medial frontal control of temporal processing in the dorsomedial striatum. *J. Neurosci.* **37**, 8718–8733.

61. Gámez, J., Mendoza, G., Prado, L., Betancourt, A. & Merchant, H. (2019). The amplitude in periodic neural state trajectories underlies the tempo of rhythmic tapping. *PLoS Biology* vol. 17.

62. Matell, M. S. & Meck, W. H. (2004). Cortico-striatal circuits and interval timing: Coincidence detection of oscillatory processes. *Cogn. Brain Res.* **21**, 139–170.

63. Kononowicz, T. W. & van Wassenhove, V. (2016). In Search of Oscillatory Traces of the Internal Clock. *Front. Psychol.* **7**, 1–5.

64. Oprisan, S. A., Dix, S. & Buhusi, C. V. (2014). Phase resetting and its implications for

interval timing with intruders. *Behav. Processes* **101**, 146–153.

65. Leon, M. I. & Shadlen, M. N. (2003). Representation of Time by Neurons in the Posterior Parietal Cortex of the Macaque. *Neuron* **38**, 317–327.

66. Meirhaeghe, N., Sohn, H. & Jazayeri, M. (2021). A precise and adaptive neural mechanism for predictive temporal processing in the frontal cortex. *Neuron* **109**, 2995-3011.e5.

67. Plenz, D. (2003). When inhibition goes incognito: Feedback interaction between spiny projection neurons in striatal function. *Trends Neurosci.* **26**, 436–443.

68. Mendez, J. C., Prado, L., Mendoza, G. & Merchant, H. (2011). Temporal and spatial categorization in human and non-human primates. *Front. Integr. Neurosci.* **5**, 1–10.

69. Jazayeri, M. & Shadlen, M. N. (2010). Temporal context calibrates interval timing. *Nat. Neurosci.* **13**, 1020–1026.

70. Gibbon, J., Church, R. M. & Meck, W. H. (1984). Scalar Timing in Memory. *Ann. N. Y. Acad. Sci.* **423**, 52–77.

1354

1355

A

Monkey#1

Sets	Caudate	Putamen	Hippocampus
1s-long	23/63 *(36.51%)*	15/55 *(27.28%)*	**15/75 *(20%)****
2s-long	**50/116 *(43.1%)****	**40/139 *(28.78%)****	**30/220 *(13.64%)****
4s-long	11/39 *(28.21%)*	16/74 *(21.62%)*	19/130 *(14.62%)*
8s-long	20/54 *(37.04%)*	26/78 ***(33.33%)****	16/68 *(23.53%)*

Monkey#2

Sets	Caudate	Putamen	Hippocampus
1s-long	36/133 *(27.07%)*	14/144 *(11.11%)*	**16/271 *(5.9%)****
2s-long	**98/345 *(28.41%)****	**51/435 *(11.72%)****	**32/537 *(5.96%)****
4s-long	39/165 *(23.64%)*	26/259 *(10.04%)*	18/210 *(8.58%)*
8s-long	33/116 *(28.45%)*	25/161 ***(15.53%)****	18/135 *(13.33%)*

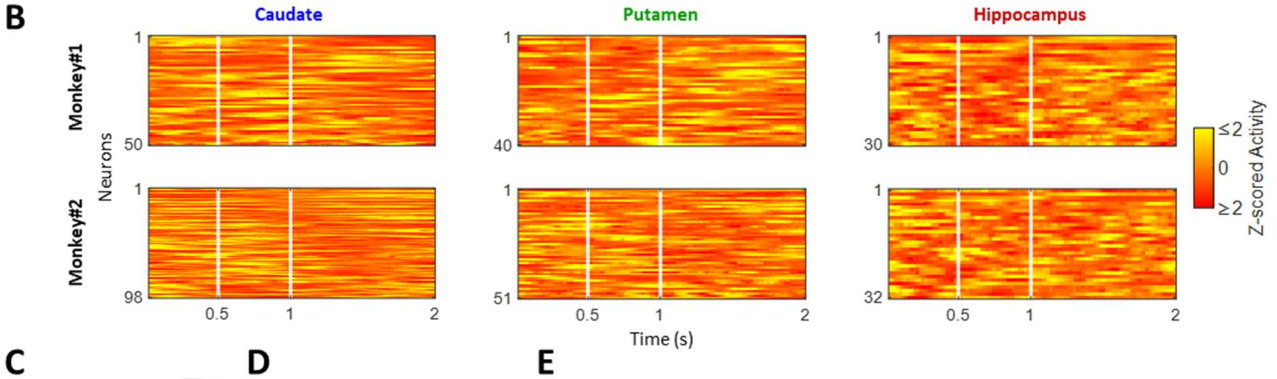

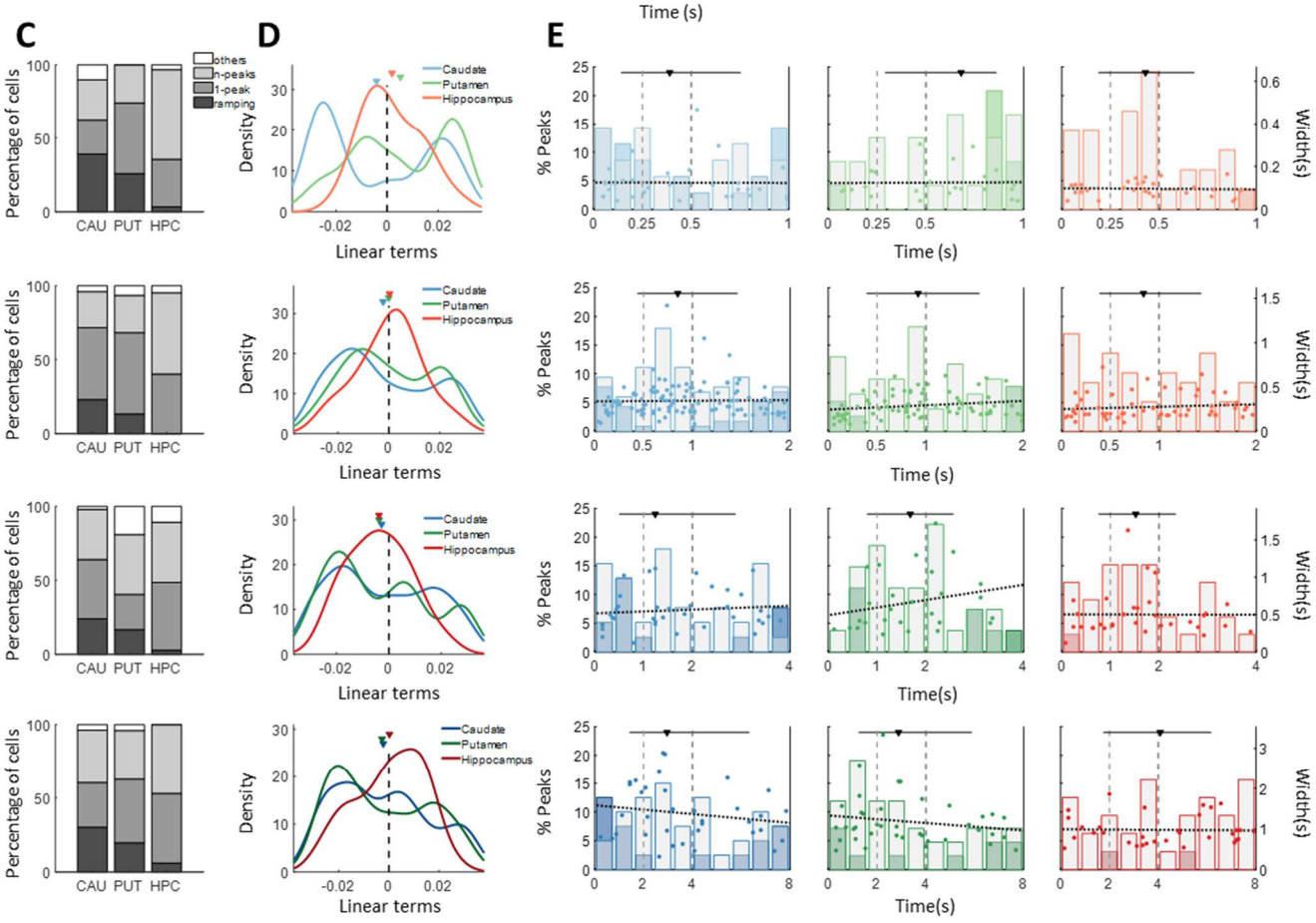

F

	Caudate (n=148)			Putamen (n=91)			Hippocampus (n=62)		
	responsive (%)	interval selective		responsive (%)	interval selective		responsive (%)	interval selective	
cue	49 (33.1)	1	short	29 (31.9)	4	short	18 (29)	0	short
		1	inter.		3	inter.		2	inter.
		1	long		0	long		1	long
total		3			7			3	
tar.	125 (84.5)	22	short	71 (78)	9	short	36 (58)	4	short
		15	inter.		13	inter.		9	inter.
		25	long		15	long		4	long
total		62			37			17	
mov.	124 (83.8)	19	short	76 (83.5)	13	short	32 (51.6)	0	short
		16	inter.		12	inter.		7	inter.
		20	long		11	long		5	long
total		55			36			12	
rew.	121 (81.8)	9	short	67 (73.6)	9	short	33 (53)	4	short
		9	inter.		10	inter.		5	inter.
		17	long		7	long		4	long
total		35			26			13	

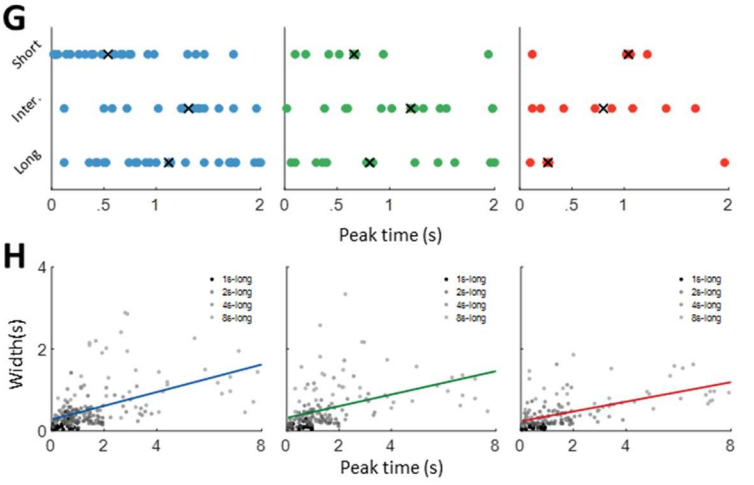

Figure S1. Population measures across regions and ranges. Related to Figure 2. A. Table showing the percentage of TM cells in each region at each time range for each monkey separately. Different proportions between monkeys are shown in bold and with an asterisk. **B.** Heatmaps of TM cells populations in Monkey#1 (top row) and in Monkey#2 (bottom row) in caudate (left column), putamen (middle column) and hippocampus (right column). Neurons are z-scored and sorted by their linear terms. Monkey#1 consistently had a higher proportion of TM cells compared to Monkey#2. However, due to the limited number of animals, it is challenging to establish a direct link between these differences and behavioural variations. **C.** Proportion of ramping cells, 1-peak, multi-peaks and other cells for each brain region across sets, from top to bottom, at sets 1s-long, 2s-long, 4s-long, 8s-long. **D.** Distribution of the linear terms obtained from the stepwise regression analysis, for each brain region across sets, from top to bottom, at sets 1s-long, 2s-long, 4s-long, 8s-long. **E.** From top to bottom, peak times at set 1s-long, 2s-long, 4s-long and 8s-long. Columns from left to right: caudate, putamen, hippocampus. Left y-axis, percentage of peak times over the interval (white bars represent peak neurons, coloured bars ramping neurons). Median of the distribution (triangle) and interquartile range represent the peaks distribution. In the caudate, the peak times were mainly distributed within the first half of the interval (medians respectively at 39, 42.5, 31, and 37% of the intervals at sets 1s-, 2s-, 4s- and 8s-long). In the putamen, the peaks were distributed in the second half of the interval at set 1s-long (median at 68%) and in the first half of the interval for the other sets (medians respectively 46, 42, and 36% of the intervals for sets 2s-, 4s- and 8s-long). In the hippocampus, peak distributions were also mainly distributed within the first half of the intervals (medians respectively at 43, 42, 38, and 51% of the interval). These observations show that overall, neurons peaked during the first half of the interval to be timed. Right y-axis shows the width size of peaks as a function of peak times. Superposed dashed line represents the fit obtained after linear regressions. None of them was significant, suggesting that the time-field of each neuron (width) did not increase linearly as a function of its peak time within the interval. **F.** Table showing the number of TM cells responding to other epochs of the task and the number of TM cells selective for an epoch of the task as a function of the length of the interval (short, intermediate, or long) for set 2s-long only. To test it, we used a LMM (see STAR Methods). A large proportion of TM cells in all regions also responded to cue, target onset, response execution and reward delivery. These proportions were higher in the striatum compared to the hippocampus. Some cells also

showed a selectivity to the trial type. **G.** Distribution of peak times during the interval as a function of neurons selectivity to short, intermediate, and long trials (bold in E) during target task epoch in set 2s-long. Crosses represent the mean peak time. From left to right: caudate, putamen and hippocampus. We found no difference in the distribution of the peaks during the long interval between 'short-preferring' neurons, 'intermediate-preferring' neuron, or 'long-preferring' neurons whether their selectivity was assessed for target presentation. motor execution or reward delivery. In sum, these results show that the neurons displayed activity outside the interval, but that this activity was not firmly indicative of the peaks' distribution within the interval. **H.** Width size of the "time-field" as a function of peak time per caudate (left), putamen (middle) and hippocampus (right) across all time ranges. Coloured lines represent the fit model of the linear regression ($\beta1= 0.168$ for caudate, $\beta1=0.1424$ for putamen and $\beta1=0.119$ for hippocampus, $p<0.0001$ in all regions).

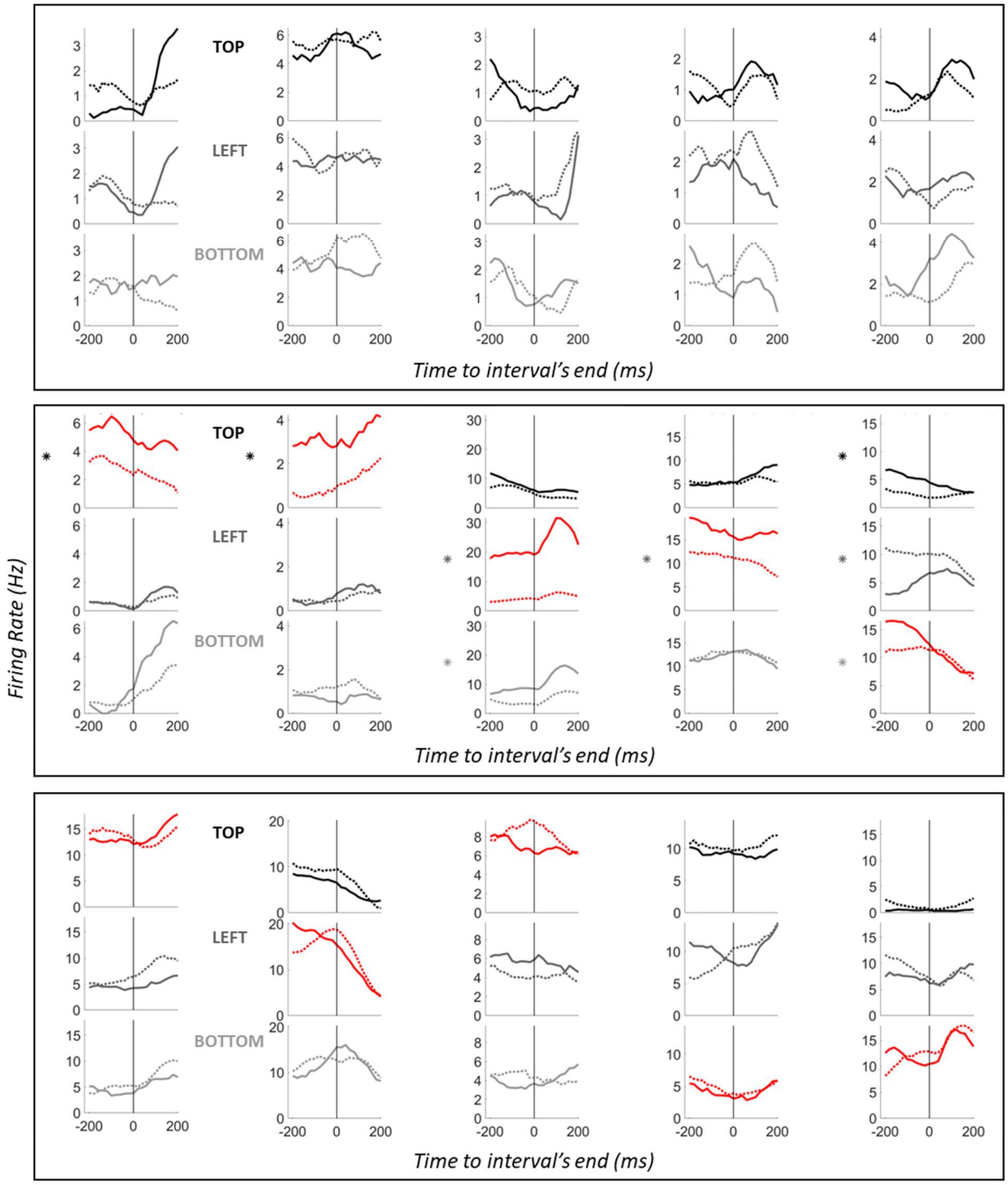

Figure S2. Single cells examples aligned at the end of the sub-second and second ranges intervals. Related to Figure 2.

Single cells activity aligned at the interval's end (target presentation). Each cell (columns) is displayed three times: before long interval's end (top movement, in black), before intermediate interval's end (left movement, dark grey) and before short interval's end (bottom movement, light grey). Analysis was performed on the 200ms before interval's end

(0 in the figure). Top row. Neurons that were not affected by time range nor following movement. Middle row. Neurons that were sensitive to both, movement and time range. “Preferred” movement is shown in red, significant pairwise comparisons following significant interaction, are shown by the asterisk. Bottom row. Neurons that were sensitive only to movement, preferred movement is shown by the red activity.

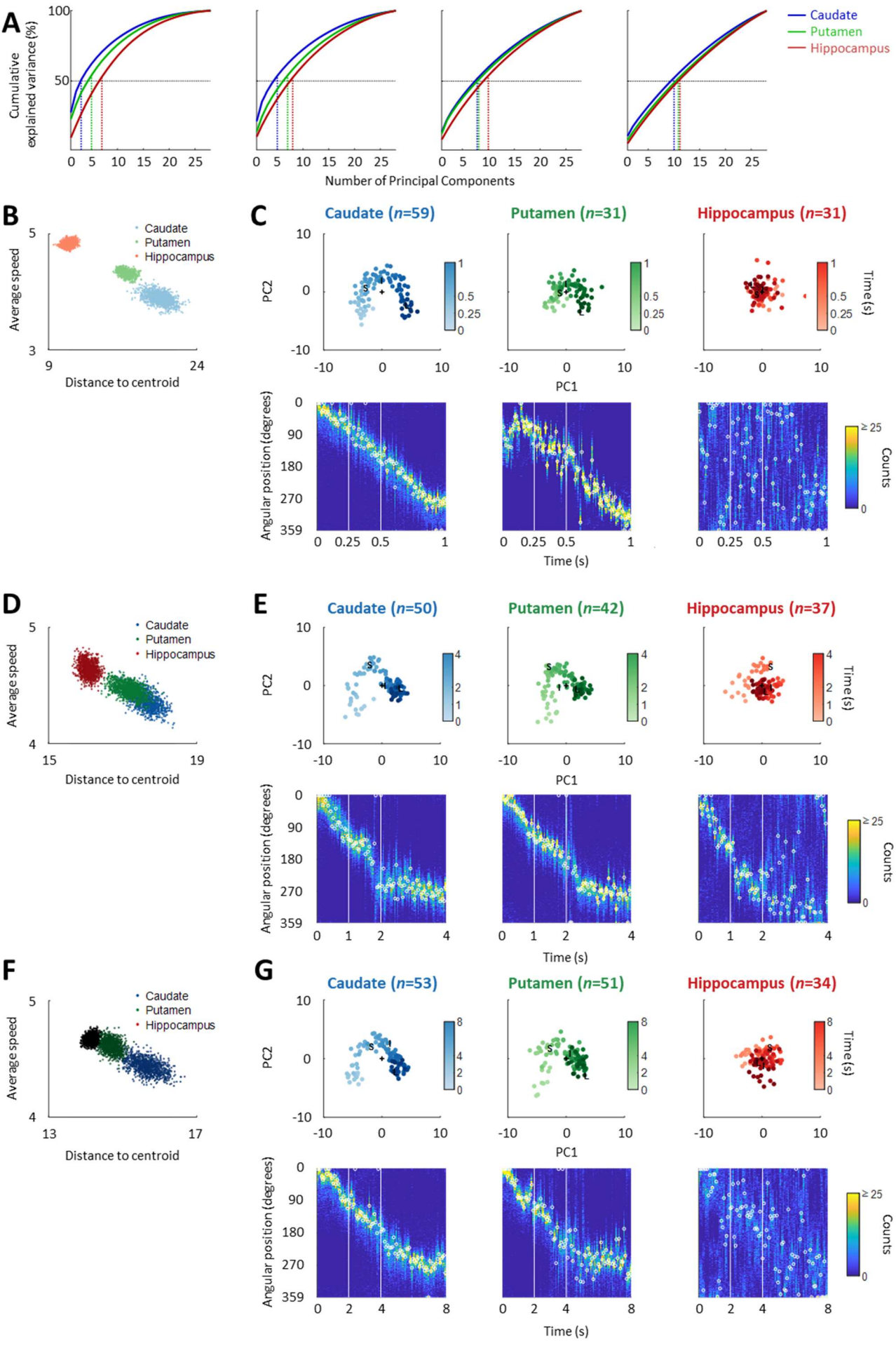
A
Cumulative explained variance (%)
Number of Principal Components
Caudate
Putamen
Hippocampus
B
Average speed
Distance to centroid
C
Caudate (n=59)
Putamen (n=31)
Hippocampus (n=31)
PC2
PC1
Time (s)
Angular position (degrees)
Counts
D
E
Caudate (n=50)
Putamen (n=42)
Hippocampus (n=37)
F
G
Caudate (n=53)
Putamen (n=51)
Hippocampus (n=34)

Figure S3. Principal Component Analysis for retiming ranges. Related to Figure 3

A. Cumulative explained variance (y-axis) as a function of Principal Components (x-axis) for each brain region (coloured lines) across time ranges, from left to right, using an absolute 20ms binning on raw data. 50% of the variance is shown by the dotted line. **B.** Average speed (y-axis) of the neural trajectories during the 1s-long interval, obtained with the first 11 PCs, from each iteration, with the down-sampling method (*i*=1000) plotted against the average distance to the centroid of the same trajectories (x-axis). **C.** Top row. Population activity over time during set 1s-long, projected onto the first two Principal Components for the caudate (left), putamen (middle), and hippocampus (right). The time of expected interval ends are indicated for short (S), intermediate (I) and long (L) intervals. The centroid of the distribution is represented with a cross. Bottom row. Distribution of angular positions computed from each iteration (*i*=1000) at each time-point for set 1s-long. White circles indicate the angle obtained the most out of the 1000 iterations, for each time-point. Time of expected interval ends are indicated with white vertical lines. **C.** Same as in A for set 4s-long. **D.** Same as in B for set 4s-long. **E.** Same as in A for set 8s-long. **F.** Same as in B for set 8s-long.

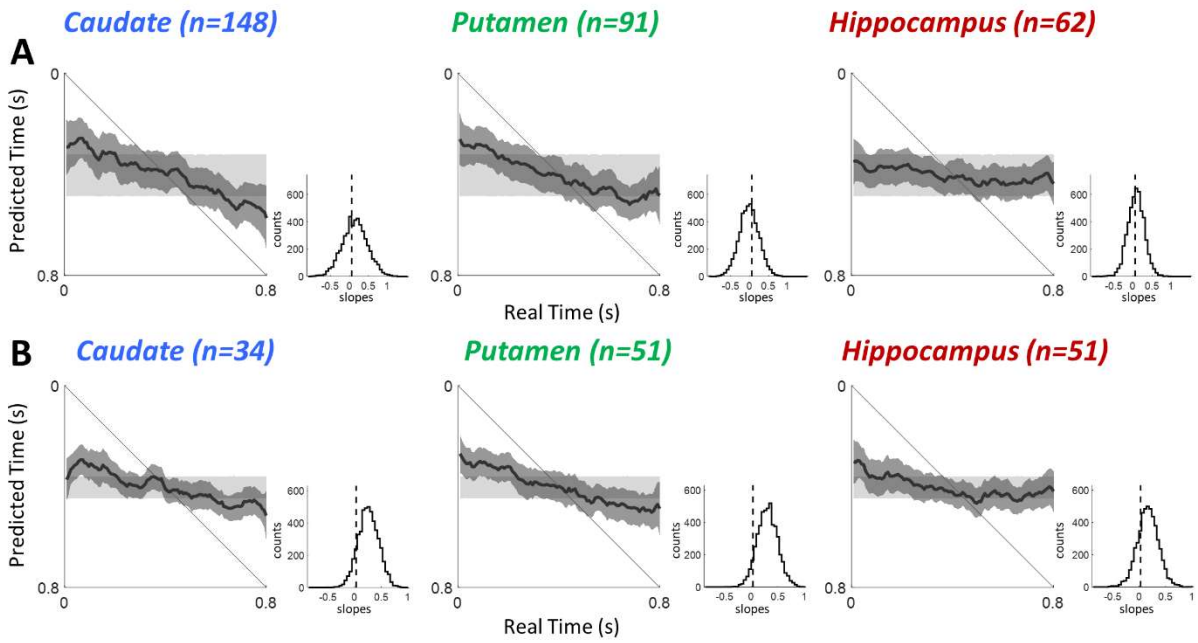

Figure S4. Absence of time decoding from inter-trial interval. Related to Figure 5

A. Multiclass decoding trained and tested on baseline activity during the ITI (black line). Decoding of predicted time (y-axis) as a function of real time (x-axis) for caudate (left), putamen (middle) and hippocampus (right). Chance value is shown with grey shade. Bottom panel. Slopes distribution obtained from the 5000 decoding outputs on baseline activity (black line) did not differ from chance. **B.** Same as in A with TM cells defined during the ITI.

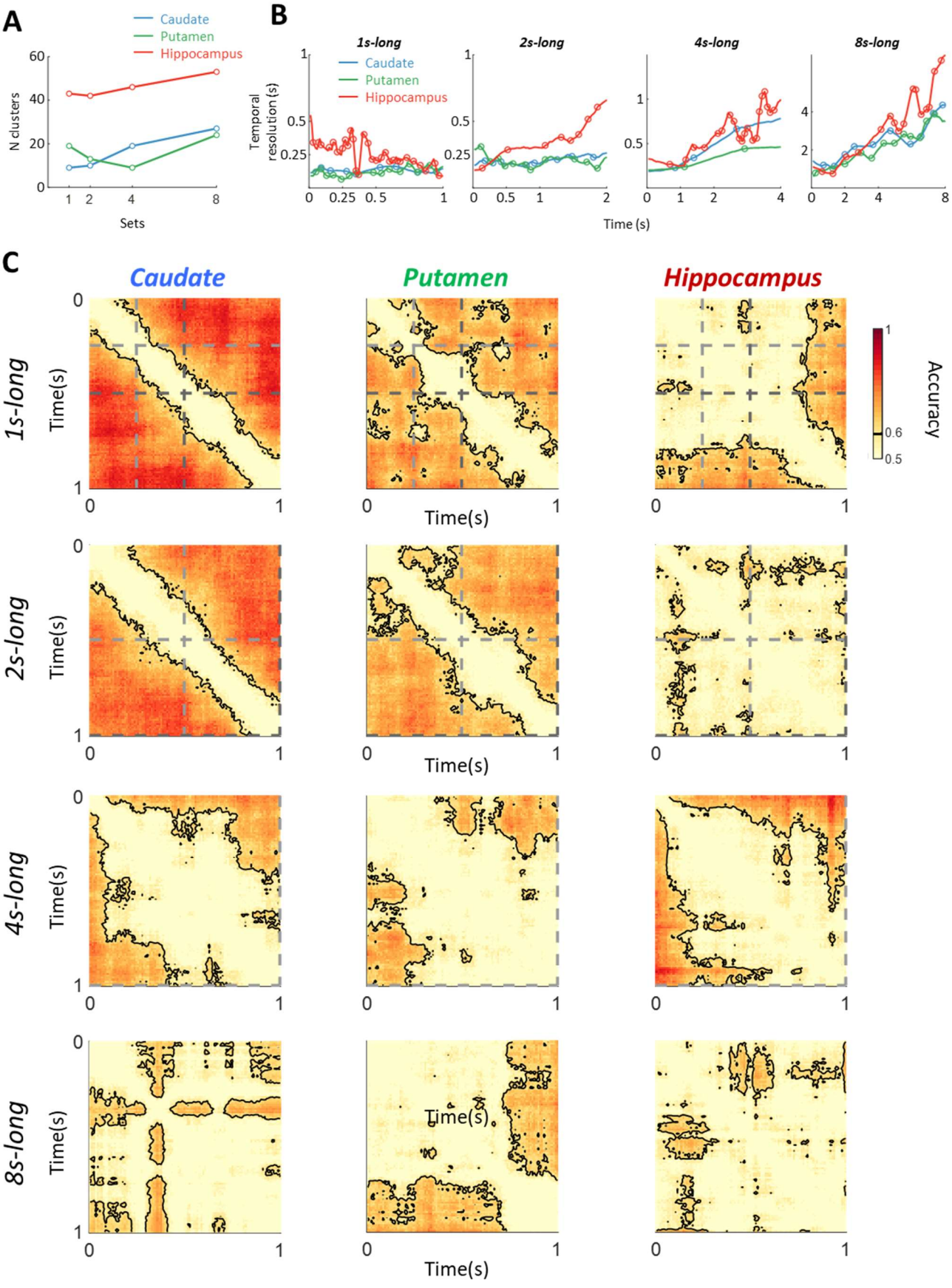
A
Caudate
Putamen
Hippocampus
N clusters
Sets
B
1s-long
2s-long
4s-long
8s-long
Temporal resolution (s)
Time (s)
C
Caudate
Putamen
Hippocampus
1s-long
2s-long
4s-long
8s-long
Time(s)
Accuracy

Figure S5. Temporal resolution of time decoding across time ranges and Time-by-time discrimination within 1s. Related to Figure 6

A. Number of clusters obtained per each brain area across time-ranges. **B.** Resolution of the temporal discrimination (y-axis) as a function of time for the 3 brain areas (caudate in blue, putamen in green and hippocampus in red). Circles show the times where the linearity of the resolution changes. From left to right: results for set 1s-long, 2s-long, 4s-long and 8s-long. **C.** Pairwise decoding computed on the neurons defined as TM cells within the first second of each interval, across different time ranges: from top to bottom are sets 1s-long, 2s-long, 4s-long and 8s-long. Brain regions are presented in columns: caudate (left), putamen (middle) and hippocampus (right). Possible times for the interval to end are represented by light grey (short) and dark grey (intermediate) dashed vertical lines. Results are displayed in a time-by-time matrix, each data-point is the discriminability accuracy between t(x) and t(y). Accuracy scores ranged from 0.5 to 1. Chance level is defined at 0.6. The temporal resolution is the window within the diagonal between black lines (chance level).